

Discovery of BMS-986202: A Clinical Tyk2 Inhibitor that Binds to Tyk2 JH2

Chunjian Liu,* James Lin, Charles Langevine, Daniel Smith, Jianqing Li, John S. Tokarski, Javed Khan, Max Ruzanov, Joann Strnad, Adriana Zupa-Fernandez, Lihong Cheng, Kathleen M. Gillooly, David Shuster, Yifan Zhang, Anil Thankappan, Kim W. McIntyre, Charu Chaudhry, Paul A. Elzinga, Manoj Chiney, Anjaneya Chimalakonda, Louis J. Lombardo, John E. Macor, Percy H. Carter, James R. Burke, and David S. Weinstein



Cite This: *J. Med. Chem.* 2021, 64, 677–694



Read Online

ACCESS |



Metrics & More

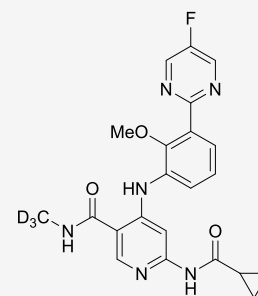


Article Recommendations



Supporting Information

ABSTRACT: A search for structurally diversified Tyk2 JH2 ligands from **6** (BMS-986165), a pyridazine carboxamide-derived Tyk2 JH2 ligand as a clinical Tyk2 inhibitor currently in late development for the treatment of psoriasis, began with a survey of six-membered heteroaryl groups in place of the *N*-methyl triazolyl moiety in **6**. The X-ray co-crystal structure of an early lead (**12**) revealed a potential new binding pocket. Exploration of the new pocket resulted in two frontrunners for a clinical candidate. The potential hydrogen bonding interaction with Thr599 in the pocket was achieved with a tertiary amide moiety, confirmed by the X-ray co-crystal structure of **29**. When the diversity search was extended to nicotinamides, a single fluorine atom addition was found to significantly enhance the permeability, which directly led to the discovery of **7** (BMS-986202) as a clinical Tyk2 inhibitor that binds to Tyk2 JH2. The preclinical studies of **7**, including efficacy studies in mouse models of IL-23-driven acanthosis, anti-CD40-induced colitis, and spontaneous lupus, will also be presented.



7 (BMS-986202)
 a clinical Tyk2 inhibitor that binds to Tyk2 JH2

INTRODUCTION

Tyrosine kinase 2 (Tyk2) is a non-receptor tyrosine kinase belonging to the Janus kinase (Jak) family that also includes Jak1, Jak2, and Jak3. Jak family members regulate immunomodulatory cytokine-initiated signaling by phosphorylating their receptors, which in turn leads to recruitment and phosphorylation of signal transducer and activation of transcription (STAT) proteins to affect the Jak-STAT-dependent transcription and functional responses.^{1–5} These cytokine signaling pathways play key roles in the pathogenesis of autoimmune and inflammatory disorders. The pursuit of Jak inhibitors as therapeutic agents has so far resulted in five FDA-approved drugs. They are pan-Jak inhibitor tofacitinib,^{6,7} Jak1/2 dual inhibitors ruxolitinib^{8,9} and baricitinib,^{10,11} moderately selective Jak1 inhibitor upadacitinib,^{12,13} and moderately selective Jak2 inhibitor fedratinib.^{14,15} For the Tyk2 specific Tyk2-STAT signaling, the involved cytokines include the p40-containing IL-12 and IL-23 as well as Type I interferon IFN α , which are implicated in diseases such as psoriasis,^{16–20} systemic lupus erythematosus (SLE),^{21–23} and inflammatory bowel disease (IBD).^{24,25} Intervening in the Tyk2-STAT signaling pathway by targeting these cytokines with biologics has been proved to be a feasible therapeutic solution to autoimmune and inflammatory diseases. For example, ustekinumab, a human IL-12/23 monoclonal antibody, was

approved by FDA for the treatment of psoriasis,²⁶ Crohn's diseases,²⁷ and ulcerative colitis.²⁸ Anifrolumab, a human monoclonal antibody that binds to and blocks Type I interferons, was shown to be efficacious in the treatment of SLE in phase III clinical trials recently.²⁹ Meanwhile, genetic studies have shown that Tyk2-deficient mice were resistant to collagen-induced arthritis (CIA) and experimental autoimmune encephalomyelitis (EAE),^{30,31} while deactivating mutations in the Tyk2 gene could provide protection from multiple autoimmune disorders including psoriasis, rheumatoid arthritis (RA), and SLE.³² As a result, Tyk2, a key regulator of the Tyk2-STAT cascade, is rationalized to be a promising small molecule target for developing orally active therapeutic agents for autoimmune and inflammatory disorders.^{33–35}

A characteristic feature of Tyk2 and other Jak family members is that they possess a canonical catalytic kinase domain and a pseudokinase domain proximal to each other.^{36,37} The catalytic kinase and pseudokinase domains

Received: September 28, 2020

Published: December 28, 2020



are also called Jak homology 1 (JH1) and Jak homology 2 (JH2), respectively. The catalytic domains of all the Jak family members have a high degree of homology, and as a result, identification of highly selective JH1 inhibitors has proven to be challenging. This is evident by the fact that the five aforementioned FDA-approved Jak inhibitor drugs, all being Jak JH1 inhibitors, consist of one pan-Jak inhibitor, two Jak1/2 dual inhibitors, one moderately selective Jak1 inhibitor, and one moderately selective Jak2 inhibitor. Severe side effects observed during clinical studies prevented the FDA from approving more efficacious higher doses for tofacitinib⁶ and baricitinib¹⁰ for the treatment of rheumatoid arthritis (RA). Also, baricitinib¹⁰ and upadacitinib¹² each carry a boxed warning, the most serious warning the FDA issues, for risks of serious infection, malignancy, and thrombosis. The adverse effects of these drugs may be linked to the lack of specificity or selectivity. Tyk2 JH1 inhibitors such as 1,³⁸ 2,³⁹ 3 (PF-06700841),^{40,41} and 4 (PF-06826647)⁴² (Figure 1) have been

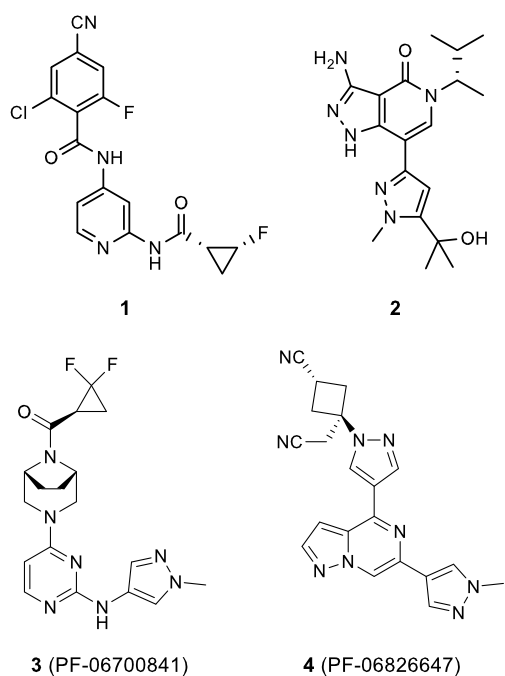


Figure 1. Literature Tyk2 JH1 inhibitors.

reported, with 3 and 4 in clinical trial phases II and I, respectively. Like the JH1 inhibitors of other Jak family members, these inhibitors are only modestly selective as they also show significant activities against other Jak family members. Our strategy to selectively target the Tyk2-STAT signaling pathway takes advantage of Tyk2 JH2. Overall, Tyk2 JH2 closely resembles Tyk2 JH1, but there are some unique differences in the binding pockets between the two domains,^{37,43} which may be sufficient for identification of Tyk2 JH2 selective inhibitors. A good indication is that Tyk2 JH2 only binds adenosine triphosphate (ATP) very weakly with a K_d of 24 μM .³⁷ Comparison of the crystal structures of Tyk2 JH2,^{37,44} Jak1 JH2,⁴⁵ and Jak2 JH2⁴⁶ also reveals unique differences in the binding pockets among these pseudokinase domains. The weak ATP binding of Tyk2 JH2 did not demonstrate any catalytic activity. However, it has been shown by mutation studies that Tyk2 JH2 plays an important

regulatory role in Tyk2 function,⁴⁷ suggesting that Tyk2 JH2 can be a druggable target.⁴⁸

We previously reported Tyk2 JH2 ligands that were remarkably selective and effective in blocking the activation of Tyk2 JH1.⁴³ Then, with compound 5 (Figure 2), an

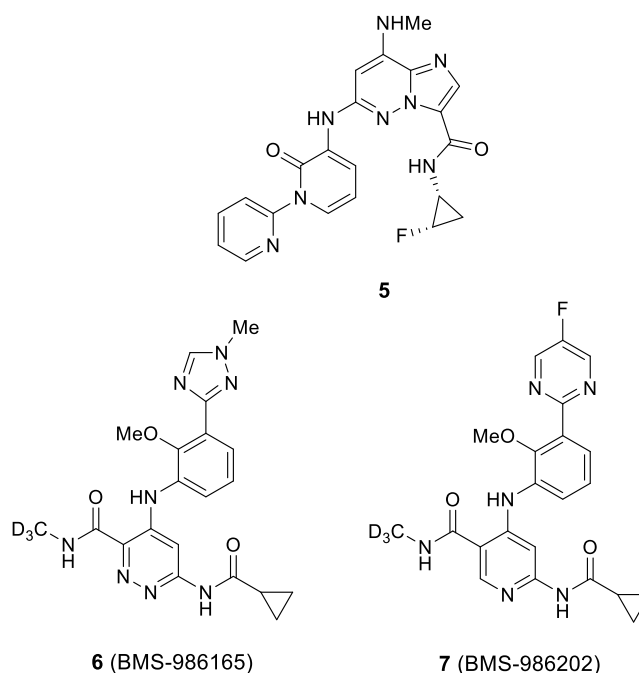


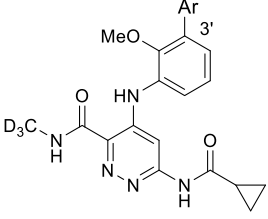
Figure 2. Tyk2 JH2 ligands as Tyk2 inhibitors.

imidazopyridazine derivative, we demonstrated the proof of concept for the idea that a small molecule Tyk2 JH2 ligand could serve as an orally active therapeutic agent for autoimmune and inflammatory diseases.⁴⁹ Most recently, we disclosed pyridazine carboxamide-based Tyk2 JH2 ligand 6 (BMS-986165) as a Tyk2 inhibitor that is currently in phase III clinical development for the treatment of psoriasis.^{50–52} Now, we present the identification and preclinical studies of a nicotinamide-derived clinical Tyk2 JH2 binding Tyk2 inhibitor 7 (BMS-986202).

RESULTS AND DISCUSSION

Structure–Activity Relationship (SAR) Studies, Lead Optimization, and X-ray Co-crystal Structures. To search for structurally differentiated Tyk2 JH2 ligands, we first investigated if the *N*-methyl triazolyl group in 6 could be replaced with a six-membered heteroaryl group. As shown in Table 1, the use of 2-pyridyl in place of the *N*-methyl triazolyl group in 6 resulted in analog 8, which turned out to be 8-fold less active than 6 against the Tyk2 pseudokinase. The compound was also less potent in the IFN α stimulated luciferase reporter assay^{49,53} in Kit225 T cells and in the IFN α stimulated STAT5 phosphorylation human whole blood (hWB) assay^{49,53} by 8- and 24-fold, respectively. Compounds 9–12 are isomeric analogs derived from the replacement of *N*-methyl triazolyl in 6 with pyridazinyl, pyrimidinyl, and pyrazinyl groups. They displayed comparable activities to one another in the Tyk2 JH2 enzymatic, cellular, and hWB assays. Compared to 8, their hWB activities were shown to be 2- to 8-fold more potent, though their enzymatic and cellular activities were about the same or only 2- to 3-fold better. Table

Table 1. SAR Observed for Ar with 8–12



compd	Ar	Tyk2 JH2 IC ₅₀ (nM) ^a	IFN α IC ₅₀ (nM) ^a	hWB IC ₅₀ (nM) ^a	h/r/mL stab. (%) ^d
6		0.20	5.3	18	98/100/89
8		1.6	41 ^b	430 ^c	79/34/42
9		1.4	69 ^b	183 ^b	60/8/0
10		1.3	20	113	48/3/3
11		0.50	29	87	58/1/1
12		0.48	17	53	100/77/78

^aMean values are determined from at least three experiments unless otherwise noted. ^bMean values determined from two experiments. ^cValue determined from one experiment. ^dPercentage remaining after 10 min of incubation in microsomes.

1 also contains the liver microsomal (LM) stability data for 8–12. Clearly, 12 was the early standout from this six-membered heteroaryl group survey as it was not only the most potent analog but also the only one that was found to be stable in liver microsomes. As a result, 12 was chosen for further SAR studies. On the other hand, two issues were identified for 12. First, though it showed an encouraging pharmacokinetic profile, improvement was needed. Second, 12 was associated with poor aqueous solubility (<1 $\mu\text{g}/\text{mL}$ at pH 6.5).

We were able to quickly obtain an X-ray co-crystal structure of 12 with the Tyk2 JH2 protein.⁵⁴ As indicated in Figure 3a, the key binding interactions between 12 and Tyk2 JH2 include (1) hydrogen bonds between the cyclopropane carboxamide NH and the carbonyl groups of Val690 as well as between a N atom of the pyridazine core and the NH group of Val690 at the hinge region, (2) a hydrogen bond between the pyridazine carboxamide NH and the carbonyl groups of Glu688, (3) a hydrogen bonding network involving the pyridazine carboxamide carbonyl group, the methoxy oxygen group, and Lys642, (4) a hydrogen bond between a N atom of pyrimidine and a NH group of Arg738, and (5) a unique hydrophobic interaction of the methoxy group with a shallow hydrophobic pocket (shown with a gray surface representation). In addition to the key binding interactions, the co-crystal structure also revealed a large empty pocket at the end of pyrimidine ring of 12 (Figure 3b). It was also noticed that, on the pocket surface, Thr599 with OH and NH groups available for potential hydrogen bond formation is within an accessible distance (~ 5 Å).

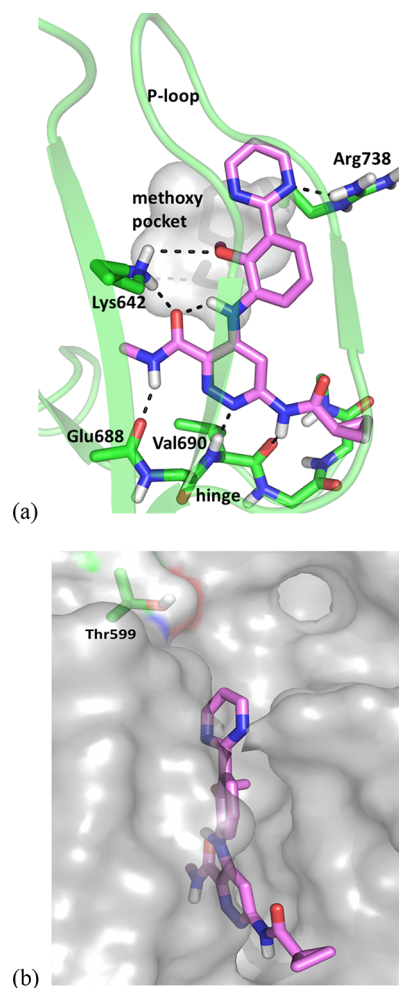
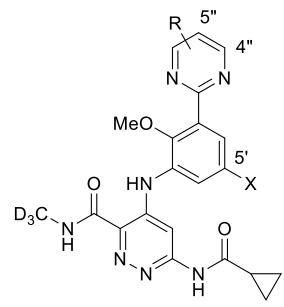


Figure 3. X-ray co-crystal structure of 12 bound to Tyk2 JH2 (PDB 7K7O). (a) Binding interaction highlights. (b) Surface representation of the Tyk2 JH2 protein showing a pocket available at the top of the pyrimidine ring.

We decided to explore the potential of the new pocket. As expected, small substitutions such as Me, F, and OMe at the 5'-position (13–15) were tolerated (Table 2), but they provided no advantages over 12. Compared to the 5'-substitutions, the 4''-substitutions (16 and 17) were less tolerated or detrimental. We next explored some bulkier, more hydrophilic functionalities such as tertiary carbinol (18) and amide (19) moieties to take advantage of the new pocket and address the poor aqueous solubility observed for 12, with the hope of also making interactions with Thr599. Analogs 18 and 19 turned out to be highly potent against Tyk2 JH2 enzymatic, cellular, and hWB assays. Also, 18 did show a significantly improved aqueous solubility of 14 $\mu\text{g}/\text{mL}$ at pH 6.5, while the aqueous solubility for 19 was not determined. However, unfortunately, both 18 and 19 displayed very poor Caco-2 permeability of 24 nm/s. Attempts to improve the permeability by using more hydrophobic carbinol (20) or amide (21) moieties were unsuccessful. We also introduced a F substituent on the aniline phenyl in 18 and 19, but the resulting analogs 22 and 23 did not show any improvement in permeability.

Continuing to search for ways to improve the permeability for 18 and 19, we prepared analogs 24 and 25, where a pyrazine ring was employed in place of the pyrimidine ring (Table 3). We rationalized that pyrazine analogs 24 and 25

Table 2. SAR Observed for R and X with 12–23

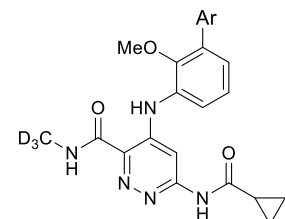


C	R	X	Tyk2 JH2 IC ₅₀ (nM) ^a	IFN α IC ₅₀ (nM) ^a	hWB IC ₅₀ (nM) ^a	Caco-2 A to B (nm/sec)
12	H	H	0.48	17	53	339
13	5''-Me	H	1.2	13 ^b	130 ^b	427
14	5''-F	H	1.9	32	163	443
15	5''-OMe	H	0.25	13 ^b	92 ^b	339
16	4''-Me	H	4.5	68	226	328
17	4''-OMe	H	1.4	50 ^b	461	248
18		H	< 0.25	9.0	41	24
19		H	< 0.25	7.6	54	24
20		H	0.44	8.6	53	16
21		H	< 0.25 ^c	8.5 ^c	42 ^c	34
22		F	0.51 ^c	18 ^c	73 ^c	20
23		F	0.52	10 ^b	47 ^b	22

^aMean values are determined from at least three experiments unless otherwise noted. ^bMean values determined from two experiments. ^cValue determined from one experiment.

should be less polar and more permeable than pyrimidine analogs **18** and **19**. To our satisfaction, **24** and **25** displayed much improved Caco-2 values of 146 and 98 nm/s, respectively. What is more, in sharp contrast to early pyrazine analog **11**, compounds **24** and **25** were found to be stable in liver microsomes. For example, after 10 min of incubation of **24** in human, rat, and mouse liver microsomes, the parent **24** was detected to be 95%, 90%, and 99%, respectively. These data may suggest that the 5''-position of the pyridinyl in **11** be a metabolic soft spot. With respect to activity, **24** appeared slightly less potent than **18**, while **25** slightly more potent than **19** in the hWB assay. Replacement of the pyrimidine ring in **18** and **19** with a pyridine ring led to **26** and **27**, which showed moderately improved permeability. The pyridazine analogs **28** and **29** were also synthesized, but they did not provide much improvement in permeability. It should be pointed out that, compared to the unsubstituted pyridinyl (**8**), pyridazinyl (**9**), and pyrazinyl (**11**) compounds (Table 1), the corresponding tertiary amide moiety containing analogs **27**, **29**, and **25** (Table 3) consistently showed improved activities in all the three

Table 3. SAR Observed for Ar with 24–29



compd	Ar	Tyk2 JH2 IC ₅₀ (nM) ^a	IFN α IC ₅₀ (nM) ^a	hWB IC ₅₀ (nM) ^a	Caco-2 A to B (nm/sec)
24		0.30	14	70	146
25		< 0.25	6.2	24	98
26		0.48	12	107	73
27		< 0.25	14	42	66
28		0.71	16	63	26
29		< 0.25	11	44	45

^aMean values are determined from at least three experiments.

assays. We were able to obtain an X-ray co-crystal structure of **29** bound to the Tyk2 JH2 protein (Figure 4), which confirmed a hydrogen bond interaction between the tertiary amide carbonyl O in **29** and the Thr599 hydroxyl H.⁵⁵

For further structural diversity away from **6**, we also examined nicotinamide analogs and found that nicotinamide

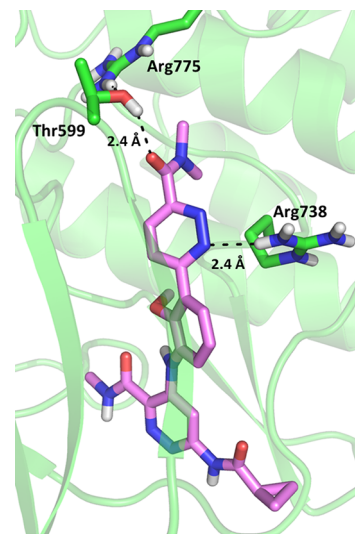
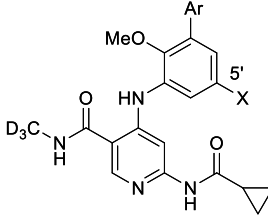


Figure 4. X-ray co-crystal structure of **29** bound to Tyk2 JH2 (PDB 7K7Q).

30 (Table 4) was at least as potent as its pyridazine carboxamide counterpart **12**. Subsequent profiling showed

Table 4. SAR Observed for Ar and X with 30–33 and 7



compd	Ar	X	Tyk2 JH2 IC ₅₀ (nM) ^a	IFN α IC ₅₀ (nM) ^a	hWB IC ₅₀ (nM) ^a	Caco-2 A to B (nm/sec)
30		H	< 0.25	6.4	41	42
31		H	0.27	29	233	32
32		H	0.54	30	341	187
7		H	0.19	10	58	96
33		F	0.25	17	59	113

^aMean values are determined from at least three experiments.

that **30** had an aqueous solubility of 32 $\mu\text{g/mL}$, significantly better than that (<1 $\mu\text{g/mL}$) for **12**. However, **30** was much less permeable compared to **12** as it displayed a Caco-2 value of 42 nm/s versus 339 nm/s for **12**. To improve the permeability for **30**, we tried the same strategy that successfully addressed the issue for pyridazine carboxamides **18** and **19**, namely, replacing the pyrimidine ring in **30** with a pyrazine ring. However, in this case, the resulting analogs **31** and **32** displayed reduced activities in the cellular and hWB assays, though compound **32** did show a significantly enhanced permeability of 187 nm/s. Fortunately, it was later found that the permeability of **30** could sufficiently be improved by introducing a single F atom to the molecule. The fluoro group could be added to the 5'-position of the pyrimidine ring or to the 5'-position of the aniline phenyl group. The resulting analogs **7** and **33** displayed a Caco-2 permeability of 96 and 113 nm/s, respectively, while largely maintaining the Tyk2 JH2 enzymatic, cellular, and hWB activities observed for **30**.

Pharmacokinetic (PK) Studies. In the course of SAR explorations, a number of analogs were advanced to full PK studies in mouse based on activities and other profiling data. The results from **12**, **24**, **25**, and **7** are arranged in Table 5. As mentioned earlier, **12**, the early pyridazine carboxamide lead directly identified from the SAR survey of six-membered heteroaryl groups in place of the *N*-methyl triazole ring in **6** displayed an encouraging PK profile with its oral exposure (AUC_{0-24h}) of 15 $\mu\text{M}\cdot\text{h}$ (when dosed at 10 mpk) and bioavailability (F%) of 31%, but improvements were desired.

Table 5. Mouse PK Profiles for 12, 24, 25, and 7^{a,b,c}

compd	12	24	25	7
PO dose (mg/kg)	10	10	10	10
C _{max} (μM)	5.4	6.1	7.8	13
AUC _{0-24 h} ($\mu\text{M}\cdot\text{h}$)	15	26	19	65
CL (mL/min/kg)	7.9	5.3	7.6	3.0
V _{ss} (L/kg)	2.3	3.4	1.5	1.1
F (%)	31	41	43	62

^aIV dose: 1 mpk. ^bIV vehicle: 20% water:80% PEG 400. ^cPO vehicle: 5:5:90 TPGS:EtOH:PEG300.

Compounds **24** and **25** were obtained from the exploration of the new binding pocket, and both showed moderately improved PK profiles, compared to **12**. However, more significant improvements were achieved with nicotinamide **7** as it increased the oral exposure by 4 times and doubled the bioavailability, compared to **12**. As a result, **7** was further studied for its PK properties in rat, cyno, and dog (Table 6),

Table 6. PK Profiles for 7 in Rat, Cyno, and Dog^{a,a,c}

species	rat	cyno	dog
PO dose (mg/kg)	10	7	10
C _{max} (μM)	13	11	14
AUC _{0-24 h} ($\mu\text{M}\cdot\text{h}$)	77	130	126
CL (mL/min/kg)	3.6	2.3	1.8
V _{ss} (L/kg)	1.1	1.7	1.5
F (%)	72	~100	~100

^aIV dose: 1 mpk for rat, 2 mpk for cyno and dog. ^bIV vehicle: 20% water:80% PEG 400. ^cPO vehicle: 5:5:90 TPGS:EtOH:PEG300.

and its exposure and bioavailability were further improved in these species, with the bioavailability reaching to 100% in cyno and dog. Across the board, the compound was shown to be of low clearance rate and low volume of distribution.

Pharmacodynamic (PD) and Efficacious Studies of 7.

To evaluate its PD responses, inhibitor **7** was tested for its ability to inhibit IL-12/IL-18-induced IFN γ production in mice. The compound was first orally dosed to mice. One and 2 h later, the animals were challenged with IL-12 and IL-18, respectively. Five hours after drug administration, plasma samples were collected and analyzed for IFN γ levels. As shown in Figure 5, compound **7** dose-dependently inhibited IFN γ production by 46% and 80% at doses of 2 and 10 mpk, respectively.

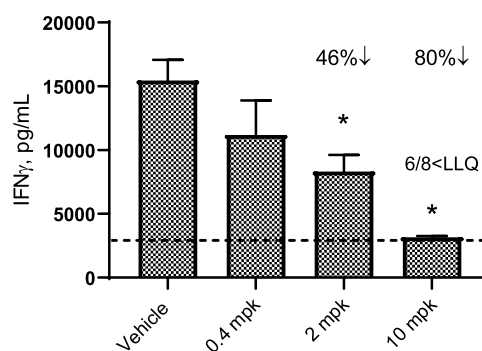


Figure 5. Inhibitor **7** in a mouse PD model of IL-12/IL-18-induced IFN γ production (vehicle: 5:5:90 EtOH:TPGS:PEG300).

For efficacy evaluations in disease models, 7 was studied in a mouse skin inflammation (psoriasis-like) model of IL-23-driven acanthosis. In this study, IL-23 was injected to mice every other day during a period of 12 days to induce acanthosis. Inhibitor 7 was orally dosed to mice once a day for the same period, with the first dose approximately 2 h prior to the first injection of IL-23. The mouse ear thickness was measured periodically and calculated for the percent change in thickness from the baseline measurement taken before the initial IL-23 injection. Ustekinumab, a human anti-IL-23 antibody was used as a positive control in the study. As shown in Figure 6, 7 inhibited ear swelling in a dose-responsive manner, with a dose of 30 mpk (QD) showing at least equivalent efficacy to ustekinumab.

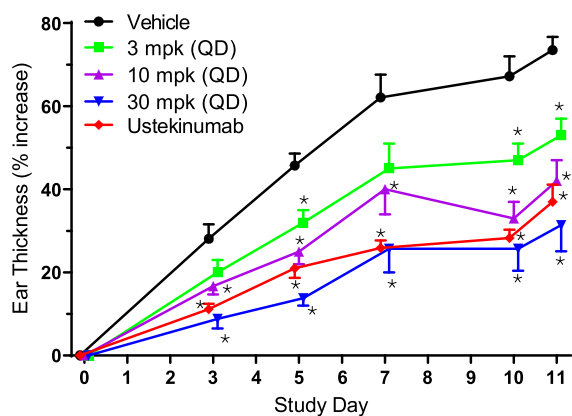


Figure 6. Inhibitor 7 in a mouse model of IL-23-driven acanthosis (QD dosing; vehicle: 5:5:90 TPGS:EtOH:PEG300).

Inhibitor 7 was also studied in the SCID mouse model of anti-CD40-induced colitis. The compound was orally dosed to SCID mice once a day for 6 days. Immediately after the first dose, the mice were challenged with a single injection of an anti-CD40 antibody to induce colitis. On day 6, all animals were euthanized for histological evaluations. An anti-p40-antibody was used as a positive control in this study. The colon histology score indicated that 7 was effective in inhibiting colitis in a dose-dependent manner, with doses of 25 and 60 mpk showing equivalent efficacy to the anti-p40 antibody (Figure 7).

Lastly, 7 was evaluated in a 12 week, spontaneous lupus model in NZB/W mice. NZB/W mice are a type of New

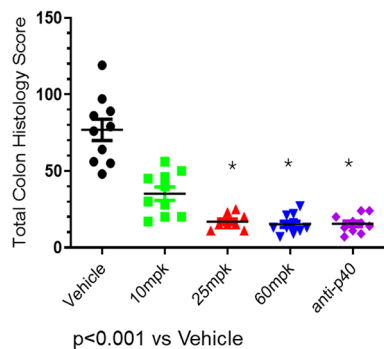


Figure 7. Inhibitor 7 in the SCID mouse model of anti-CD40-induced colitis (QD dosing; vehicle: aqueous suspension containing 0.5% Methocel and 0.1% Tween-80).

Zealand black and white hybrid mice. These mice will spontaneously develop an autoimmune syndrome similar to that of lupus patients, characterized by high levels of antinuclear antibodies and proteinuria, and therefore can be used as a lupus model without needing any challenges.⁵⁶ Compound 7 was orally dosed to NZB/W mice at the age of 23 weeks or so, when no severe proteinuria was detected, once a day for 12 weeks. The anti-dsDNA titers and proteinuria were measured periodically. In this study, mouse anti-interferon receptor antibody MAR1-5A3 was used as a positive control. As shown in Figure 8, Tyk2 JH2 ligand 7 dose-dependently suppressed the level of anti-dsDNA titers and prevented proteinuria development.

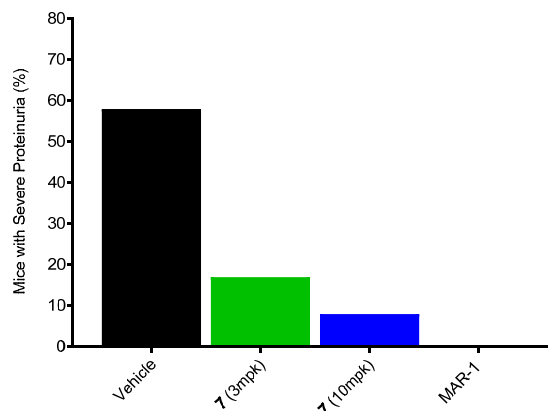
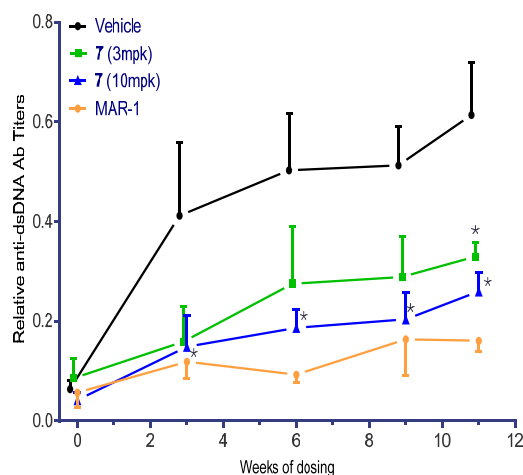


Figure 8. Inhibitor 7 in a spontaneous lupus model in NZB/W mice (QD dosing; vehicle: 5:5:90 EtOH:TPGS:PEG300).

Additional Profiling Data of 7. Extensive profiling was completed for 7, and some of the data are arranged in Table 7. As shown earlier, 7 and many other analogs were extremely active against our Tyk2 JH2 enzymatic assay, and we believed that the enzymatic assay might be beyond its capability to determine the true IC_{50} values for those compounds. As a result, for important analogs, we also obtained their K_i values by Morrison titration.⁴⁹ For 7, the Tyk2 JH2 IC_{50} was measured to be 0.19 nM, but its K_i was determined to be 0.02 nM. In addition to the IFN α stimulated luciferase reporter assay^{49,53} in Kit225 T cells, we also had an IL-23 stimulated reporter assay (in Kit225 T cells)⁵³ against which the cellular activity (IL-23 IC_{50}) of 7 was determined to be 12 nM, almost

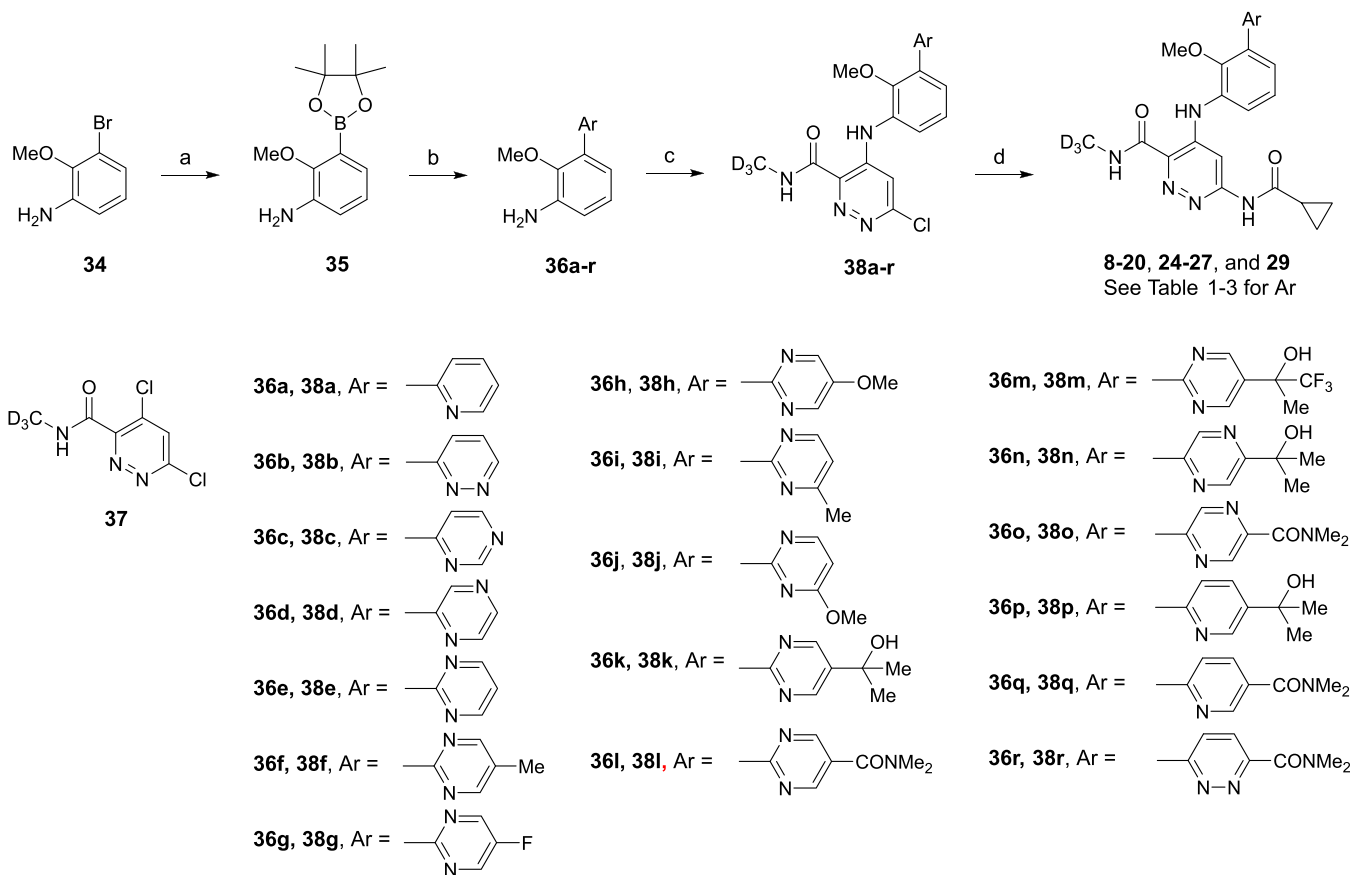
Table 7. *In vitro* Profile of 7

assays	results
Tyk2 JH2 IC ₅₀ (nM)	0.19
Tyk2 JH2 Ki (nM)	0.02
IFN α IC ₅₀ (nM)	10
IL-23 IC ₅₀ (nM)	12
hWB IC ₅₀ (nM)	58
mWB IC ₅₀ (nM)	481
liver microsomal half-life (min)	>120 in mouse, rat, monkey, and humans; 89 in dog
Caco-2 A to B (nm/s)	96
Serum protein binding (%)	92.4 (h), 96.0 (r), 93.3 (m), 94.1 (c), 89.3 (d)
P450 IC ₅₀ (μ M)	>40 for 1A2, 3A4, 2B6, 2C9, 2D6; 14 for 2C19
kinase selectivity	>10,000-fold over 273 kinases and pseudokinases, JAK1 JH2 IC ₅₀ = 7.8 nM, IL-2 IC ₅₀ (Jak1/3-dependent cellular activity): >12.5 μ M, EPO IC ₅₀ (Jak2-dependent cellular activity): >10 μ M

identical to what was obtained from the IFN α stimulated cellular assay. In addition to the hWB assay, 7 was also evaluated in a mWB assay.⁵³ It was found that 7 was 8-fold less potent in the mWB assay than in the hWB assay. Given the efficacy observed in multiple mouse disease models, this human/mouse WB potency discrepancy only made us feel

more confident about the prospects for the compound in patients. The 8-fold discrepancy between the hWB and mWB potency is also consistent with what was observed for 6 (BMS-986165). Inhibitor 7 is stable in liver microsomes, with half lives of greater than 120 min in mouse, rat, monkey, and humans and 89 min in dog. The serum protein binding for 7 in these species ranges from 89.3% to 96.0%, leaving a good range of free fraction of drug available. Compound 7 did not inhibit cytochrome P450 isozymes 1A2, 3A4, 2B6, 2C9, 2C19, and 2D6 with IC₅₀ values less than 40 μ M, but it was a weak inhibitor of 2C19 with an IC₅₀ of 14 μ M. The compound proved to be exquisitely selective over other kinases, displaying >10,000-fold selectivity for Tyk2 JH2 over a diverse panel of 273 kinases and pseudokinases that include Jak family members. Compound 7 did bind Jak1 JH2 with an IC₅₀ of 7.8 nM, but this enzymatic binding did not lead to any functional activities as 7 displayed an activity (IC₅₀) of greater than 12.5 μ M in the IL-2 stimulated Jak1/3-dependent cellular assay. The compound was also shown to display an activity (IC₅₀) of greater than 10 μ M in the EPO-stimulated Jak2-dependent TF-1 cell assay. In short, the profiling studies did not reveal liabilities for 7, and the compound ultimately passed the preclinical toxicity studies to advance to clinical studies.

Chemistry. The syntheses of pyridazine carboxamides 8–20, 24–27, and 29 are outlined in Scheme 1. Reaction of 3-bromo-2-methoxyaniline (34) with 4,4,4',4',5,5,5',5'-octa-

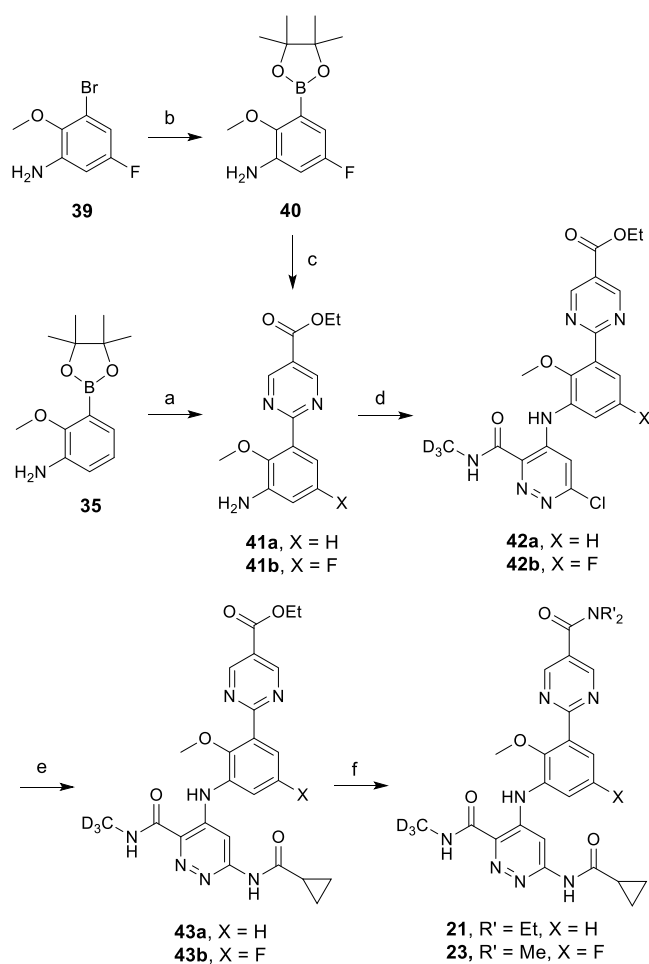
Scheme 1. Synthesis of 8–20, 24–27, and 29^a

^aReagents and conditions: (a) 4,4,4',4',5,5,5',5'-octamethyl-2,2'-bi(1,3,2-dioxaborolane), PdCl₂(dppf)-CH₂Cl₂, KOAc, 1,4-dioxane, 110 °C, 20 h, 60%; (b) ArCl, PdCl₂(dppf)-CH₂Cl₂, K₃PO₄, 1,4-dioxane, 110 °C, 31–82%; (c) 37, LiN(SiMe₃)₂, THF, rt, 7–92%; (d) cyclopropanecarboxamide, Pd₂(dba)₃, XantPhos, Cs₂CO₃, 1,4-dioxane, 145 °C, 6–56%.

methyl-2,2'-bi(1,3,2-dioxaborolane) in the presence of [1,1'-bis(diphenylphosphino)ferrocene]dichloropalladium(II), complex with dichloromethane ($\text{PdCl}_2(\text{dppf})\text{-CH}_2\text{Cl}_2$) supplied dioxaborolane **35**. Suzuki coupling reaction of **35** and heteroaryl halide (ArCl), commercially available or readily prepared using literature procedures, gave rise to aniline **36a–r**. Treatment of **36a–r** with 4,6-dichloro-*N*-(methyl- d_3)-pyridazine-3-carboxamide (**37**), a previously reported key intermediate,⁵³ and lithium bis(trimethylsilyl)amide regioselectively provided precursor **38a–r**. Buchwald coupling reaction of **38a–r** and cyclopropanecarboxamide, effected by tris(dibenzylideneacetone)dipalladium(0) ($\text{Pd}_2(\text{dba})_3$) and 4,5-bis(diphenylphosphino)-9,9-dimethylxanthene (XantPhos), afforded analogs **8–20**, **24–27**, and **29**.

The syntheses of **21** and **23** are shown in Scheme 2. Suzuki reaction of **35** and ethyl 2-chloropyrimidine-5-carboxylate

Scheme 2. Synthesis of **21** and **23**^a



^aReagents and conditions: (a) ethyl 2-chloropyrimidine-5-carboxylate, $\text{PdCl}_2(\text{dppf})\text{-CH}_2\text{Cl}_2$, K_3PO_4 , 1,4-dioxane, 75 °C, 74%; (b) 4,4',4'',5,5',5''-octamethyl-2,2'-bi(1,3,2-dioxaborolane), $\text{PdCl}_2(\text{dppf})\text{-CH}_2\text{Cl}_2$, K_2OAc , 1,4-dioxane, 105 °C, 61%; (c) ethyl 2-chloropyrimidine-5-carboxylate, $\text{PdCl}_2(\text{dppf})\text{-CH}_2\text{Cl}_2$, K_3PO_4 , 1,4-dioxane, 75 °C, 79%; (d) **37**, $\text{LiN}(\text{SiMe}_3)_2$, THF, rt, 32% and 43% for **42a** and **42b**, respectively; (e) cyclopropanecarboxamide, $\text{Pd}_2(\text{dba})_3$, XantPhos, Cs_2CO_3 , 1,4-dioxane, 150 °C, microwave, 72% and 50% for **43a** and **43b**, respectively; (f) i. $\text{LiOH}\cdot\text{H}_2\text{O}$, MeOH/THF , rt; ii. Et_2NH or Me_2NH , BOP, (*i*-Pr)₂NEt, THF, 50 °C, 12% and 42% over two steps for **21** and **23**, respectively.

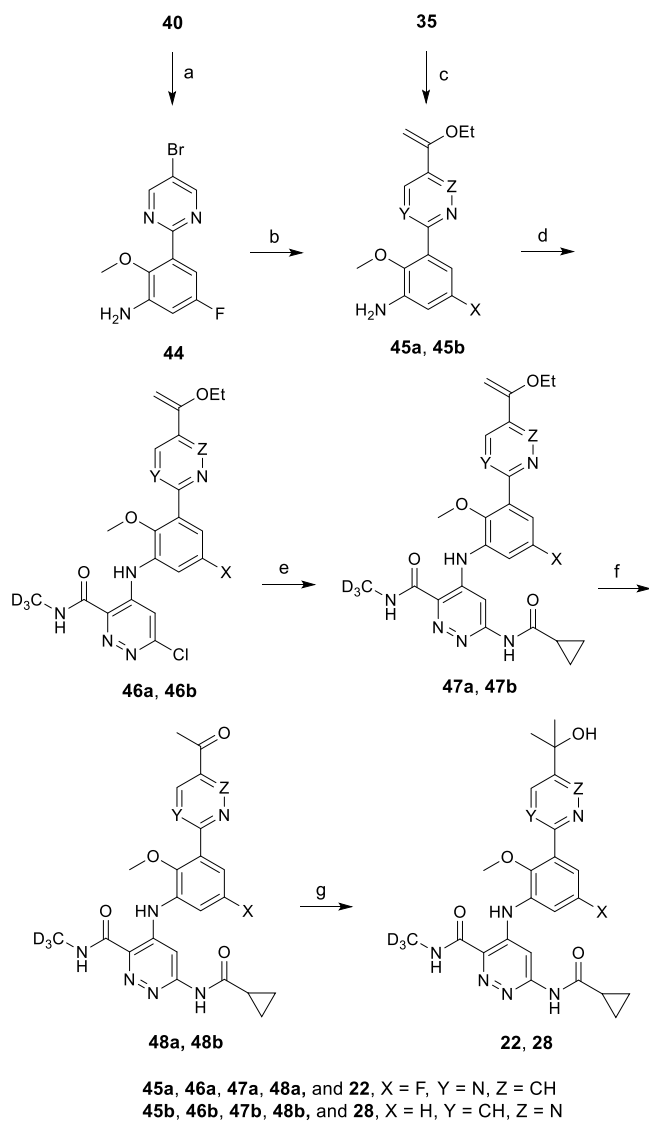
provided aniline **41a**. To avoid significant hydrolysis of the ester functionality, it was important to run the reaction at a relatively low temperature (75 °C) and within a relatively short period of time (4 h). In the same manner, **41b** was obtained from **40**, which was prepared from 3-bromo-5-fluoro-2-methoxyaniline (**39**). Treatment of **41a** and **41b** with 4,6-dichloro-*N*-(methyl- d_3)-pyridazine-3-carboxamide (**37**)⁵³ in the presence of lithium bis(trimethylsilyl)amide resulted in chloropyridazine carboxamides **42a** and **42b**, which were then converted to **43a** and **43b** by Buchwald reaction. Hydrolysis of **43a** and **43b** with lithium hydroxide, followed by an amide formation coupling reaction, furnished analogs **21** and **23**.

Analog **22** and **28** were synthesized according to Scheme 3. Bromopyrimidine **44** was obtained from **40**, via Suzuki reaction, and transformed to vinyl ether **45a** with tributyl(1-ethoxyvinyl)stannane and $\text{Pd}(\text{PPh}_3)_2\text{Cl}_2$. Meanwhile, vinyl ether **45b** was prepared from **35** and commercially available 3-chloro-6-(1-ethoxyvinyl)pyridazine. Reaction of **45a** and **45b** with 4,6-dichloro-*N*-(methyl- d_3)-pyridazine-3-carboxamide (**37**)⁵³ and lithium bis(trimethylsilyl)amide led to the formation of **46a** and **46b**, which were then reacted with cyclopropanecarboxamide in the presence of $\text{Pd}_2(\text{dba})_3$ and XantPhos to yield **47a** and **47b**. Vinyl ether **47a** and **47b** were converted to methyl ketone **48a** and **48b** with 1 N hydrochloric acid. Treatment of **48a** and **48b** with methylmagnesium bromide provided targets **22** and **28**.

Nicotinamides **7** and **30–33** were synthesized (Scheme 4) in a similar manner as pyridazine carboxamides **8–20**, **24–27**, and **29** were (Scheme 1), except that now 4,6-dichloro-*N*-(methyl- d_3)-nicotinamide (**49**)⁵³ was employed in place of 4,6-dichloro-*N*-(methyl- d_3)-pyridazine-3-carboxamide (**37**). Dichloronicotinamide **49** displayed the same desired regioselectivity as dichloropyridazine carboxamide **37** when reacting with anilines **36e**, **36g**, and **36s–u** in the presence of lithium bis(trimethylsilyl)amide. Also, the resulting chloronicotinamide **50a–e** behaved very similarly to their chloropyridazine carboxamide counterparts when subjected to Buchwald conditions to afford **7** and **30–33**.

CONCLUSIONS

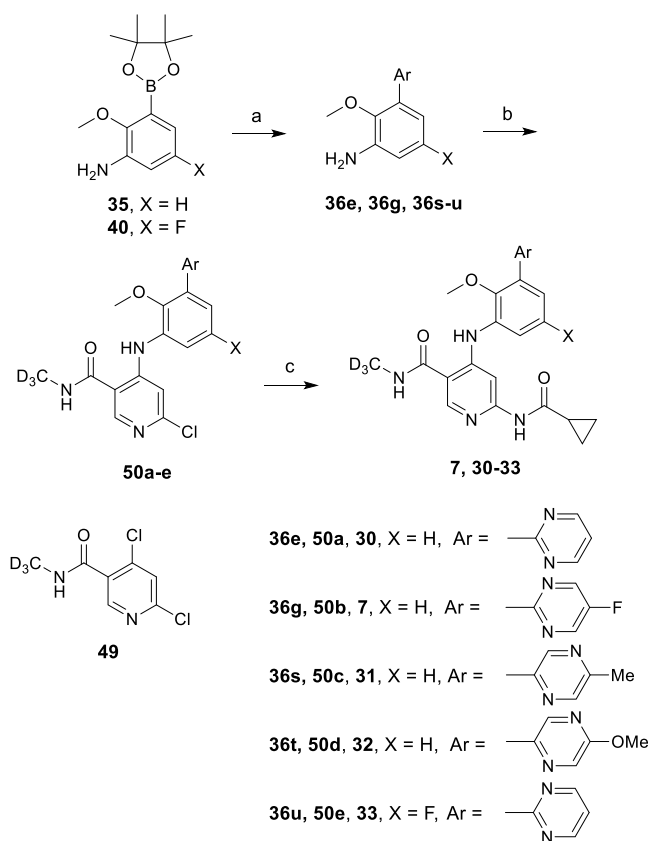
To search for structurally diversified Tyk2 inhibitors that bind to Tyk2 JH2, a SAR survey of six-membered heteroaryl groups in place of the *N*-methyl triazolyl group in **6** was conducted. Interestingly, the X-ray co-crystal structure of an early lead (**12**) from this survey revealed a potential new binding pocket. Exploration of this potential pocket resulted in compounds with improved potency, properties, and PK profiles, compared to the early analogs. The X-ray co-crystal structure of such an analog (**29**) showed an additional hydrogen bonding interaction with Thr599 in the pocket. In the nicotinamide series, a series that is much more polar and less permeable than the pyridazine carboxamides, it was found that introduction of a single F atom to a molecule could significantly improve the permeability. This finding directly led to the identification of **7** (BMS-986202). Tyk2 JH2 ligand **7** proved to be remarkably selective over other kinases including Jak family members. The compound dose-dependently inhibited IL-12/IL-18-induced IFN γ production in a pharmacodynamic model. It was further demonstrated that **7** was highly efficacious in three disease models: IL-23-driven acanthosis, anti-CD40-induced colitis, and spontaneous lupus.

Scheme 3. Synthesis of 22 and 28^a

^aReagents and conditions: (a) 2,5-dibromopyrimidine, PdCl₂(dppf)-CH₂Cl₂, K₃PO₄, 1,4-dioxane, 90 °C, 43%; (b) tributyl(1-ethoxyvinyl)stannane, Pd(PPh₃)₂Cl₂, Et₃N, DMF, 100 °C, 75%; (c) 3-chloro-6-(1-ethoxyvinyl)pyridazine, PdCl₂(dppf)-CH₂Cl₂, K₃PO₄, 105 °C, 1,4-dioxane, 100%; (d) 37, LiN(SiMe₃)₂, THF, rt, 75% and 52 for 46a and 46b, respectively; (e) cyclopropanecarboxamide, Pd₂(dba)₃, XantPhos, Cs₂CO₃, 1,4-dioxane, 150 °C, microwave, 71% for 47a; (f) 1 N HCl, THF, rt, 76% for 48a and 52% (over 2 steps) for 48b; (g) MeMgBr, THF, 0 °C, 29% and 38% for 22 and 28, respectively.

EXPERIMENTAL SECTION

Chemistry. All reagents were purchased from commercial sources and used without further purification unless otherwise noted. All reactions involving air- or moisture-sensitive reagents were performed under an inert atmosphere. Proton and carbon magnetic resonance (¹H and ¹³C NMR) spectra were recorded either on a Bruker Avance 400 or a JEOL Eclipse 500 spectrometer and are reported in ppm relative to the reference solvent of the sample in which they were run. HPLC and LCMS analyses were conducted using a Shimadzu LC-10AS liquid chromatograph and a SPDUV-vis detector at 220 or 254 nm with the MS detection performed with a Micromass Platform LC spectrometer. HPLC analyses were performed using the following conditions: Ballistic YMC S5 ODS 4.6 mm × 50 mm column with a binary solvent system where solvent A = 10% methanol and 90% water with 0.2% phosphoric acid and solvent B = 90% methanol and

Scheme 4. Synthesis of 7 and 30–33^a

^aReagents and conditions: (a) ArCl, PdCl₂(dppf)-CH₂Cl₂, K₃PO₄, 1,4-dioxane, 110 °C, 29–81%; (b) 49, LiN(SiMe₃)₂, THF, rt, 63–77%; (c) cyclopropanecarboxamide, Pd₂(dba)₃, XantPhos, Cs₂CO₃, 1,4-dioxane, 145 °C, 45–65%.

10% water with 0.2% phosphoric acid, flow rate = 4 mL/min, linear gradient time = 4 min. All final compounds had HPLC purity of 95% or better unless specifically mentioned. LCMS analyses were performed using the following conditions: Phenomenex 5 μm C18.4.6 mm × 50 mm column with a binary solvent system where solvent A = 10% methanol and 90% water with 0.1% trifluoroacetic acid and solvent B = 90% methanol and 10% water with 0.1% trifluoroacetic acid, flow rate = 4 mL/min, linear gradient time = 2 min. Preparative reversed-phase HPLC purifications were performed using one of the following two conditions: (1) Ballistic YMC S5 ODS 20 mm × 100 mm column with a binary solvent system where solvent A = 10% methanol and 90% water with 0.1% trifluoroacetic acid and solvent B = 90% methanol and 10% water with 0.1% trifluoroacetic acid, flow rate = 20 mL/min, linear gradient time = 10 min; (2) Waters XBridge C18, 19 × 200 mm column with a binary solvent system where solvent A = 5% acetonitrile and 95% water with 10 mM ammonium acetate and solvent B = 95% acetonitrile and 5% water with 10 mM ammonium acetate, flow rate = 20 mL/min, linear gradient time = 20 min.

2-Methoxy-3-(4,4,5,5-tetramethyl-1,3,2-dioxaborolan-2-yl)-aniline (35). A mixture of 3-bromo-2-methoxyaniline (34) (3.00 g, 14.85 mmol), 4,4,4',5,5,5'-octamethyl-2,2'-bi(1,3,2-dioxaborolane) (5.66 g, 22.27 mmol), PdCl₂(dppf)-CH₂Cl₂ adduct (0.728 g, 0.891 mmol), and potassium acetate (4.37 g, 44.5 mmol) in 1,4-dioxane (60 mL) was heated in a pressure bottle at 110 °C for 20 h. Upon cooling to rt, the mixture was diluted with ethyl acetate (60 mL) and filtered through Celite. The filtrate was concentrated under vacuum, and the residue was subjected to flash chromatography (330 g ISCO column, 0–40% ethyl acetate/hexane) to provide the title compound (2.31 g, 9.27 mmol, 62% yield) as a white solid. LCMS (ESI) *m/z* calcd for C₁₃H₂₀BNO₃ (M + H)⁺: 250.2, found: 250.3. ¹H

NMR (400 MHz, DMSO- d_6) δ 6.79–6.77 (m, 2H), 6.76–6.72 (m, 1H), 4.77 (s, 2H), 3.63 (s, 3H), 1.27 (s, 12H).

General Procedure for the Preparation of 36a–u, Exemplified by 2-(5-(3-Amino-2-methoxyphenyl)pyrazin-2-yl)propan-2-ol (36n). A mixture of 2-(5-chloropyrazin-2-yl)propan-2-ol⁵⁷ (0.1907 g, 1.105 mmol), 2-methoxy-3-(4,4,5,5-tetramethyl-1,3,2-dioxaborolan-2-yl)aniline (35) (0.2842 g, 1.015 mmol), 2 M K₃PO₄ solution (1.523 mL, 3.05 mmol), and PdCl₂(dppf)-CH₂Cl₂ adduct (0.050 g, 0.061 mmol) in 1,4-dioxane (7 mL) in a sealed pressure vial was degassed and heated at 105 °C for 20 h. After cooling to room temperature, the solution was diluted with ethyl acetate (25 mL) and filtered through Celite. The filtrate was washed with water (10 mL). The aqueous layer was extracted with ethyl acetate (2 x 25 mL). The combined organic phase was dried over Na₂SO₄ and concentrated under vacuum. The residue was subjected to flash chromatography (24 g ISCO column, 0–100% ethyl acetate/hexane) to give the title compound (0.221 g, 0.834 mmol, 82% yield) as a yellow oil. LCMS (ESI) m/z calcd for C₁₄H₁₇N₃O₂ (M + H)⁺: 260.1, found: 260.2. ¹H NMR (400 MHz, DMSO- d_6) δ 8.95 (d, J = 1.5 Hz, 1H), 8.90 (d, J = 1.6 Hz, 1H), 6.98–6.92 (m, 1H), 6.90–6.85 (m, 1H), 6.81 (dd, J = 7.8, 1.8 Hz, 1H), 5.45 (s, 1H), 5.10 (s, 2H), 3.47 (s, 3H), 1.51 (s, 6H).

2-Methoxy-3-(pyridin-2-yl)aniline (36a). Yield: 44%. LCMS (ESI) m/z calcd for C₁₂H₁₂N₂O (M + H)⁺: 201.1, found: 201.3. ¹H NMR (400 MHz, DMSO- d_6) δ 8.68–8.62 (m, 1H), 7.87–7.81 (m, 1H), 7.80–7.76 (m, 1H), 7.33 (ddd, J = 7.2, 4.8, 1.4 Hz, 1H), 6.94–6.88 (m, 1H), 6.87–6.82 (m, 1H), 6.76 (dd, J = 7.6, 1.8 Hz, 1H), 5.00 (s, 2H), 3.42 (s, 3H).

2-Methoxy-3-(pyridazin-3-yl)aniline (36b). Yield: 59%. LCMS (ESI) m/z calcd for C₁₁H₁₁N₃O (M + H)⁺: 202.1, found: 202.1. ¹H NMR (400 MHz, DMSO- d_6) δ 9.20 (dd, J = 4.8, 1.8 Hz, 1H), 7.97 (dd, J = 8.6, 1.5 Hz, 1H), 7.73 (dd, J = 8.6, 4.8 Hz, 1H), 7.04–6.94 (m, 1H), 6.87 (ddd, J = 9.9, 7.9, 1.8 Hz, 2H), 5.12 (s, 2H), 3.42 (s, 3H).

2-Methoxy-3-(pyrimidin-4-yl)aniline (36c). Yield: 59%. LCMS (ESI) m/z calcd for C₁₁H₁₁N₃O (M + H)⁺: 202.1, found: 202.2.

2-Methoxy-3-(pyrazin-2-yl)aniline (36d). Yield: 67%. LCMS (ESI) m/z calcd for C₁₁H₁₁N₃O (M + H)⁺: 202.1, found: 202.2. ¹H NMR (400 MHz, DMSO- d_6) δ 9.01 (d, J = 1.5 Hz, 1H), 8.73 (dd, J = 2.6, 1.6 Hz, 1H), 8.58 (d, J = 2.6 Hz, 1H), 7.00–6.94 (m, 1H), 6.90–6.86 (m, 1H), 6.83 (dd, J = 7.8, 1.8 Hz, 1H), 5.12 (s, 2H), 3.46 (s, 3H).

2-Methoxy-3-(pyrimidin-2-yl)aniline (36e). Yield: 81%. LCMS (ESI) m/z calcd for C₁₁H₁₁N₃O (M + H)⁺: 202.1, found: 202.2. ¹H NMR (400 MHz, DMSO- d_6) δ 8.89 (d, J = 5.1 Hz, 2H), 7.44 (t, J = 4.8 Hz, 1H), 6.96–6.88 (m, 1H), 6.86–6.80 (m, 2H), 5.00 (s, 2H), 3.63 (s, 3H).

2-Methoxy-3-(5-methylpyrimidin-2-yl)aniline (36f). Yield: 31%. LCMS (ESI) m/z calcd for C₁₂H₁₃N₃O (M + H)⁺: 216.1, found: 216.1. ¹H NMR (400 MHz, DMSO- d_6) δ 8.73 (s, 2H), 6.94–6.86 (m, 1H), 6.83–6.77 (m, 2H), 4.97 (br s, 2H), 3.61 (s, 3H), 2.32 (s, 3H).

3-(5-Fluoropyrimidin-2-yl)-2-methoxyaniline (36g). Yield: 82%. LCMS (ESI) m/z calcd for C₁₁H₁₀FN₃O (M + H)⁺: 220.1, found: 220.4. ¹H NMR (400 MHz, DMSO- d_6) δ 8.98 (d, J = 0.7 Hz, 2H), 6.96–6.88 (m, 1H), 6.86–6.79 (m, 2H), 5.03 (s, 2H), 3.62 (s, 3H).

2-Methoxy-3-(5-methoxypyrimidin-2-yl)aniline (36h). Yield: 54%. LCMS (ESI) m/z calcd for C₁₂H₁₃N₃O₂ (M + H)⁺: 232.1, found: 232.2.

2-Methoxy-3-(4-methylpyrimidin-2-yl)aniline (36i). Yield: 50%. LCMS (ESI) m/z calcd for C₁₂H₁₃N₃O (M + H)⁺: 216.1, found: 216.2.

2-Methoxy-3-(4-methoxypyrimidin-2-yl)aniline (36j). Yield: 40%. LCMS (ESI) m/z calcd for C₁₂H₁₃N₃O₂ (M + H)⁺: 232.1, found: 232.2. ¹H NMR (400 MHz, DMSO- d_6) δ 8.59 (d, J = 5.9 Hz, 1H), 6.91–6.85 (m, 3H), 6.84–6.80 (m, 1H), 5.00 (s, 2H), 3.97 (s, 3H), 3.68 (s, 3H).

2-(2-(3-Amino-2-methoxyphenyl)pyrimidin-5-yl)propan-2-ol (36k). Yield: 54%. LCMS (ESI) m/z calcd for C₁₄H₁₇N₃O₂ (M + H)⁺: 260.1, found: 260.1.

2-(3-Amino-2-methoxyphenyl)-N,N-dimethylpyrimidine-5-carboxamide (36l). Yield: 46%. LCMS (ESI) m/z calcd for C₁₄H₁₆N₄O₂ (M + H)⁺: 273.1, found: 273.2. ¹H NMR (400 MHz, chloroform- d) δ 8.88 (s, 2H), 7.22–7.15 (m, 1H), 6.97 (t, J = 7.8 Hz, 1H), 6.83 (dd, J = 7.8, 1.6 Hz, 1H), 3.90 (br s, 2H), 3.63 (s, 3H), 3.10 (br s, 3H), 3.05 (br s, 3H).

2-(2-(3-Amino-2-methoxyphenyl)pyrimidin-5-yl)-1,1,1-trifluoropropan-2-ol (36m). Yield: 47%. LCMS (ESI) m/z calcd for C₁₄H₁₄F₃N₃O₂ (M + H)⁺: 314.1, found: 314.4.

5-(3-Amino-2-methoxyphenyl)-N,N-dimethylpyrazine-2-carboxamide (36o). Yield: 71%. LCMS (ESI) m/z calcd for C₁₄H₁₆N₄O₂ (M + H)⁺: 273.1, found: 273.1.

2-(6-(3-Amino-2-methoxyphenyl)pyridin-3-yl)propan-2-ol (36p). Yield: 35%. LCMS (ESI) m/z calcd for C₁₅H₁₈N₂O₂ (M + H)⁺: 259.1, found: 259.2.

6-(3-Amino-2-methoxyphenyl)-N,N-dimethylnicotinamide (36q). Yield: 51%. LCMS (ESI) m/z calcd for C₁₅H₁₇N₃O₂ (M + H)⁺: 272.1, found: 272.1. ¹H NMR (500 MHz, chloroform- d) δ 8.80 (dd, J = 2.3, 0.9 Hz, 1H), 7.94 (dd, J = 8.2, 0.8 Hz, 1H), 7.85 (dd, J = 8.1, 2.3 Hz, 1H), 7.15 (dd, J = 7.8, 1.7 Hz, 1H), 7.06 (t, J = 7.8 Hz, 1H), 6.86 (dd, J = 7.8, 1.7 Hz, 1H), 4.19–3.74 (br s, 2H), 3.53 (s, 3H), 3.19 (br s, 3H), 3.12 (br s, 3H).

6-(3-Amino-2-methoxyphenyl)-N,N-dimethylpyridazine-3-carboxamide (36r). Yield: 72%. LCMS (ESI) m/z calcd for C₁₄H₁₆N₄O₂ (M + H)⁺: 273.1, found: 273.1.

2-Methoxy-3-(5-methylpyrazin-2-yl)aniline (36s). Yield: 59%. LCMS (ESI) m/z calcd for C₁₂H₁₃N₃O (M + H)⁺: 216.1, found: 216.2.

2-Methoxy-3-(5-methoxypyrazin-2-yl)aniline (36t). Yield: 29%. LCMS (ESI) m/z calcd for C₁₂H₁₃N₃O₂ (M + H)⁺: 232.1, found: 232.1. ¹H NMR (400 MHz, DMSO- d_6) δ 8.59 (d, J = 1.3 Hz, 1H), 8.38 (d, J = 1.3 Hz, 1H), 6.96–6.88 (m, 1H), 6.87–6.81 (m, 1H), 6.76 (dd, J = 7.7, 1.8 Hz, 1H), 5.04 (s, 2H), 3.96 (s, 3H), 3.45 (s, 3H).

5-Fluoro-2-methoxy-3-(pyrimidin-2-yl)aniline (36u). Yield: 73%. LCMS (ESI) m/z calcd for C₁₁H₁₀FN₃O (M + H)⁺: 220.1, found: 220.1. ¹H NMR (400 MHz, DMSO- d_6) δ 8.89 (d, J = 4.8 Hz, 2H), 7.46 (t, J = 5.0 Hz, 1H), 6.56 (ddd, J = 13.5, 10.1, 3.1 Hz, 2H), 5.36 (s, 2H), 3.60 (s, 3H).

General Procedure for the Preparation of 38a–r, Exemplified by 6-Chloro-4-((3-(5-(2-hydroxypropan-2-yl)pyrazin-2-yl)-2-methoxyphenyl)amino)-N-(methyl- d_3)pyridazine-3-carboxamide (38n). To a solution of 2-(5-(3-amino-2-methoxyphenyl)pyrazin-2-yl)propan-2-ol (36n) (0.219 g, 0.843 mmol) and 4,6-dichloro-N-trideuteriomethylpyridazine-3-carboxamide (37)⁵³ (0.168 g, 0.803 mmol) in THF (8 mL) at rt was added 1 M lithium bis(trimethylsilyl)amide/THF (3.21 mL, 3.21 mmol) over 1 min. The mixture was stirred at rt for 1 h before it was quenched with water (5 mL). The resulting mixture was adjusted with 1 N HCl solution to pH 9–10, diluted with ethyl acetate (125 mL), and washed with water (20 mL) and brine (20 mL) successively. The organic layer was dried over anhydrous MgSO₄ solution. The desired product (0.208 g, 0.482 mmol, 60% yield), was isolated as an off-white solid by flash chromatography (24 g ISCO column, 0–100% ethyl acetate/hexane). LCMS (ESI) m/z calcd for C₂₀H₁₈D₃ClN₆O₃ (M + H)⁺: 432.2, found: 432.2. ¹H NMR (400 MHz, DMSO- d_6) δ 11.14 (s, 1H), 9.39 (s, 1H), 9.02 (d, J = 1.5 Hz, 1H), 8.98 (d, J = 1.6 Hz, 1H), 7.72–7.61 (m, 2H), 7.38 (t, J = 7.9 Hz, 1H), 7.26 (s, 1H), 5.52 (s, 1H), 3.56 (s, 3H), 1.53 (s, 6H).

6-Chloro-4-((2-methoxy-3-(pyridin-2-yl)phenyl)amino)-N-(methyl- d_3)pyridazine-3-carboxamide (38a). Yield: 74%. LCMS (ESI) m/z calcd for C₁₈H₁₃D₃ClN₅O₂ (M + H)⁺: 373.1, found: 373.3.

6-Chloro-4-((2-methoxy-3-(pyridazin-3-yl)phenyl)amino)-N-(methyl- d_3)pyridazine-3-carboxamide (38b). Yield: 92%. LCMS (ESI) m/z calcd for C₁₇H₁₂D₃ClN₆O₂ (M + H)⁺: 374.1, found: 374.2.

6-Chloro-4-((2-methoxy-3-(pyrimidin-4-yl)phenyl)amino)-N-(methyl- d_3)pyridazine-3-carboxamide (38c). Yield: 66%. LCMS (ESI) m/z calcd for C₁₇H₁₂D₃ClN₆O₂ (M + H)⁺: 374.1, found: 374.2.

6-Chloro-4-((2-methoxy-3-(pyrazin-2-yl)phenyl)amino)-N-(methyl- d_3)pyridazine-3-carboxamide (38d). Yield: 78%. LCMS (ESI) m/z calcd for C₁₇H₁₂D₃ClN₆O₂ (M + H)⁺: 374.1, found: 374.2.

6-Chloro-4-((2-methoxy-3-(pyrimidin-2-yl)phenyl)amino)-N-(methyl-*d*₃)pyridazine-3-carboxamide (**38e**). Yield: 58%. LCMS (ESI) *m/z* calcd for C₁₇H₁₂D₃ClN₆O₂ (M + H)⁺: 374.1, found: 374.2.

6-Chloro-4-((2-methoxy-3-(5-methylpyrimidin-2-yl)phenyl)amino)-N-(methyl-*d*₃)pyridazine-3-carboxamide (**38f**). Yield: 40%. LCMS (ESI) *m/z* calcd for C₁₈H₁₄D₃ClN₆O₂ (M + H)⁺: 388.1, found: 388.1.

6-Chloro-4-((3-(5-fluoropyrimidin-2-yl)-2-methoxyphenyl)amino)-N-(methyl-*d*₃)pyridazine-3-carboxamide (**38g**). Yield: 67%. LCMS (ESI) *m/z* calcd for C₁₇H₁₁D₃ClFN₆O₂ (M + H)⁺: 392.1, found: 392.3. ¹H NMR (400 MHz, DMSO-*d*₆) δ 11.09 (s, 1H), 9.36 (s, 1H), 9.04 (s, 2H), 7.67 (dd, *J* = 7.9, 1.5 Hz, 1H), 7.58 (dd, *J* = 7.7, 1.5 Hz, 1H), 7.33 (t, *J* = 7.8 Hz, 1H), 7.18 (s, 1H), 3.65 (s, 3H).

6-Chloro-4-((2-methoxy-3-(5-methoxy-pyrimidin-2-yl)phenyl)amino)-N-(methyl-*d*₃)pyridazine-3-carboxamide (**38h**). Yield: 55%. LCMS (ESI) *m/z* calcd for C₁₈H₁₄D₃ClN₆O₃ (M + H)⁺: 404.1, found: 404.4.

6-Chloro-4-((2-methoxy-3-(4-methylpyrimidin-2-yl)phenyl)amino)-N-(methyl-*d*₃)pyridazine-3-carboxamide (**38i**). Yield: 65%. LCMS (ESI) *m/z* calcd for C₁₈H₁₄D₃ClN₆O₂ (M + H)⁺: 388.1, found: 388.3.

6-Chloro-4-((2-methoxy-3-(4-methoxy-pyrimidin-2-yl)phenyl)amino)-N-(methyl-*d*₃)pyridazine-3-carboxamide (**38j**). Yield: 47%. LCMS (ESI) *m/z* calcd for C₁₈H₁₄D₃ClN₆O₃ (M + H)⁺: 404.1, found: 404.2.

6-Chloro-4-((3-(5-(2-hydroxypropan-2-yl)pyrimidin-2-yl)-2-methoxyphenyl)amino)-N-(methyl-*d*₃)pyridazine-3-carboxamide (**38k**). Yield: 23%. LCMS (ESI) *m/z* calcd for C₂₀H₁₈D₃ClN₆O₃ (M + H)⁺: 432.2, found: 432.2.

6-Chloro-4-((3-(5-(dimethylcarbamoyl)pyrimidin-2-yl)-2-methoxyphenyl)amino)-N-(methyl-*d*₃)pyridazine-3-carboxamide (**38l**). Yield: 7%. LCMS (ESI) *m/z* calcd for C₂₀H₁₇D₃ClN₇O₃ (M + H)⁺: 445.2, found: 445.5.

6-Chloro-4-((2-methoxy-3-(5-(1,1,1-trifluoro-2-hydroxypropan-2-yl)pyrimidin-2-yl)phenyl)amino)-N-(methyl-*d*₃)pyridazine-3-carboxamide (**38m**). Yield: 83%. LCMS (ESI) *m/z* calcd for C₂₀H₁₅D₃ClF₃N₆O₃ (M + H)⁺: 486.1, found: 486.5. ¹H NMR (400 MHz, DMSO-*d*₆) δ 11.10 (s, 1H), 9.37 (s, 1H), 9.14 (s, 2H), 7.70 (dd, *J* = 7.9, 1.5 Hz, 1H), 7.65 (dd, *J* = 7.8, 1.6 Hz, 1H), 7.35 (t, *J* = 7.9 Hz, 1H), 7.19 (s, 1H), 7.13 (s, 1H), 3.70 (s, 3H), 1.83 (s, 3H).

6-Chloro-4-((3-(5-(dimethylcarbamoyl)pyrazin-2-yl)-2-methoxyphenyl)amino)-N-(methyl-*d*₃)pyridazine-3-carboxamide (**38o**). Yield: 89%. LCMS (ESI) *m/z* calcd for C₂₀H₁₇D₃ClN₇O₃ (M + H)⁺: 445.2, found: 445.1. ¹H NMR (400 MHz, DMSO-*d*₆) δ 11.17 (s, 1H), 9.40 (s, 1H), 9.09 (d, *J* = 1.5 Hz, 1H), 8.97 (d, *J* = 1.5 Hz, 1H), 7.71 (td, *J* = 7.8, 1.6 Hz, 2H), 7.41 (t, *J* = 7.9 Hz, 1H), 7.28 (s, 1H), 3.58 (s, 3H), 3.08 (s, 3H), 3.07 (s, 3H).

6-Chloro-4-((3-(5-(2-hydroxypropan-2-yl)pyridin-2-yl)-2-methoxyphenyl)amino)-N-(methyl-*d*₃)pyridazine-3-carboxamide (**38p**). Yield: 49%. LCMS (ESI) *m/z* calcd for C₂₁H₁₉D₃ClN₅O₃ (M + H)⁺: 431.2, found: 431.2. ¹H NMR (400 MHz, DMSO-*d*₆) δ 11.15 (s, 1H), 9.38 (s, 1H), 8.82 (dd, *J* = 2.3, 0.7 Hz, 1H), 7.96 (dd, *J* = 8.3, 2.4 Hz, 1H), 7.85–7.77 (m, 1H), 7.65–7.56 (m, 2H), 7.32 (t, *J* = 7.8 Hz, 1H), 7.26 (s, 1H), 5.33–5.21 (br s, 1H), 3.51 (s, 3H), 1.52 (s, 6H).

6-Chloro-4-((3-(5-(dimethylcarbamoyl)pyridin-2-yl)-2-methoxyphenyl)amino)-N-(methyl-*d*₃)pyridazine-3-carboxamide (**38q**). Yield: 70%. LCMS (ESI) *m/z* calcd for C₂₀H₁₇D₃ClN₇O₃ (M + H)⁺: 444.2, found: 444.2.

6-Chloro-4-((3-(6-(dimethylcarbamoyl)pyridazin-3-yl)-2-methoxyphenyl)amino)-N-(methyl-*d*₃)pyridazine-3-carboxamide (**38r**). Yield: 81%. LCMS (ESI) *m/z* calcd for C₂₀H₁₇D₃ClN₇O₃ (M + H)⁺: 445.2, found: 445.1.

General Procedure for the Preparation of 8–20, 24–27, and 29, Exemplified by 6-(Cyclopropanecarboxamido)-4-((3-(5-(2-hydroxypropan-2-yl)pyrazin-2-yl)-2-methoxyphenyl)amino)-N-(methyl-*d*₃)pyridazine-3-carboxamide (24). A mixture of 6-chloro-4-((3-(5-(2-hydroxypropan-2-yl)pyrazin-2-yl)-2-methoxyphenyl)amino)-N-(methyl-*d*₃)pyridazine-3-carboxamide (**38n**) (0.102 g, 0.236 mmol), cyclopropanecarboxamide (0.040 g, 0.473 mmol), XantPhos (0.021 g, 0.035 mmol), cesium carbonate (0.169 g, 0.520 mmol), and Pd₂(dba)₃ (0.032 g, 0.035 mmol) in 1,4-dioxane (5.4 mL) and *N*-methyl-2-pyrrolidinone (0.54 mL) was

heated at 145 °C under microwave conditions for 1 h. Upon cooling to rt, the mixture was diluted with ethyl acetate (10 mL) and filtered through Celite. The filtrate was concentrated under vacuum, and the residue was subjected to preparative HPLC. The correct fractions were combined, basified with solid NaHCO₃, concentrated under vacuum, and extracted with dichloromethane (3 x 30 mL). The combined extract was dried over Na₂SO₄. Removal of the solvent under vacuum provided the title compound (0.0342 g, 0.071 mmol, 30% yield) as a light yellow solid. LCMS (ESI) *m/z* calcd for C₂₄H₂₄D₃N₇O₄ (M + H)⁺: 481.2, found: 481.5. ¹H NMR (400 MHz, DMSO-*d*₆) δ 11.32 (s, 1H), 10.97 (s, 1H), 9.14 (s, 1H), 9.01 (d, *J* = 1.5 Hz, 1H), 8.96 (d, *J* = 1.5 Hz, 1H), 8.16 (s, 1H), 7.60–7.52 (m, 2H), 7.39–7.29 (m, 1H), 5.49 (s, 1H), 3.53 (s, 3H), 2.14–2.03 (m, 1H), 1.52 (s, 6H), 0.86–0.78 (m, 4H).

6-(Cyclopropanecarboxamido)-4-((2-methoxy-3-(pyridin-2-yl)phenyl)amino)-N-(methyl-*d*₃)pyridazine-3-carboxamide (**8**). Yield: 28%. LCMS (ESI) *m/z* calcd for C₂₂H₁₉D₃N₆O₃ (M + H)⁺: 422.2, found: 422.4. ¹H NMR (500 MHz, DMSO-*d*₆) δ 11.31 (s, 1H), 10.98 (s, 1H), 9.12 (s, 1H), 8.76–8.67 (m, 1H), 8.18 (s, 1H), 7.92–7.87 (m, 1H), 7.87–7.83 (m, 1H), 7.52 (td, *J* = 8.0, 1.6 Hz, 2H), 7.40 (ddd, *J* = 7.2, 4.9, 1.3 Hz, 1H), 7.31 (t, *J* = 7.9 Hz, 1H), 3.48 (s, 3H), 2.09 (quin, *J* = 6.1 Hz, 1H), 0.84 (d, *J* = 6.1 Hz, 1H).

6-(Cyclopropanecarboxamido)-4-((2-methoxy-3-(pyridazin-3-yl)phenyl)amino)-N-(methyl-*d*₃)pyridazine-3-carboxamide (**9**). Yield: 17%. LCMS (ESI) *m/z* calcd for C₂₁H₁₈D₃N₇O₃ (M + H)⁺: 423.2, found: 423.4. ¹H NMR (400 MHz, DMSO-*d*₆) δ 11.32 (s, 1H), 10.98 (s, 1H), 9.25 (dd, *J* = 5.0, 1.7 Hz, 1H), 9.13 (s, 1H), 8.16 (s, 1H), 8.04 (dd, *J* = 8.6, 1.5 Hz, 1H), 7.79 (dd, *J* = 8.6, 5.1 Hz, 1H), 7.58 (ddd, *J* = 11.5, 7.9, 1.5 Hz, 2H), 7.41–7.33 (m, 1H), 3.47 (s, 3H), 2.08 (quin, *J* = 6.2 Hz, 1H), 0.83 (d, *J* = 6.2 Hz, 1H).

6-(Cyclopropanecarboxamido)-4-((2-methoxy-3-(pyrimidin-4-yl)phenyl)amino)-N-(methyl-*d*₃)pyridazine-3-carboxamide (**10**). Yield: 46%. LCMS (ESI) *m/z* calcd for C₂₁H₁₈D₃N₇O₃ (M + H)⁺: 423.2, found: 423.3. ¹H NMR (400 MHz, DMSO-*d*₆) δ 11.34 (s, 1H), 11.00 (s, 1H), 9.32 (d, *J* = 1.2 Hz, 1H), 9.16 (s, 1H), 8.89 (d, *J* = 5.4 Hz, 1H), 8.16 (s, 1H), 8.00 (dd, *J* = 5.3, 1.4 Hz, 1H), 7.69 (dd, *J* = 7.8, 1.5 Hz, 1H), 7.62 (dd, *J* = 7.9, 1.5 Hz, 1H), 7.38 (t, *J* = 7.9 Hz, 1H), 3.56 (s, 3H), 2.09 (quin, *J* = 6.2 Hz, 1H), 0.86–0.81 (m, 4H).

6-(Cyclopropanecarboxamido)-4-((2-methoxy-3-(pyrazin-2-yl)phenyl)amino)-N-(methyl-*d*₃)pyridazine-3-carboxamide (**11**). Yield: 34%. LCMS (ESI) *m/z* calcd for C₂₁H₁₈D₃N₇O₃ (M + H)⁺: 423.2, found: 423.3. ¹H NMR (400 MHz, DMSO-*d*₆) δ 11.34 (s, 1H), 10.99 (s, 1H), 9.15 (s, 1H), 9.08 (d, *J* = 1.5 Hz, 1H), 8.80 (dd, *J* = 2.6, 1.6 Hz, 1H), 8.66 (d, *J* = 2.6 Hz, 1H), 8.17 (s, 1H), 7.58 (ddd, *J* = 7.9, 6.8, 1.5 Hz, 2H), 7.43–7.30 (m, 1H), 3.52 (s, 3H), 2.18–2.03 (m, 1H), 0.89–0.78 (m, 4H).

6-(Cyclopropanecarboxamido)-4-((2-methoxy-3-(pyrimidin-2-yl)phenyl)amino)-N-(methyl-*d*₃)pyridazine-3-carboxamide (**12**). Yield: 36%. LCMS (ESI) *m/z* calcd for C₂₁H₁₈D₃N₇O₃ (M + H)⁺: 423.2, found: 423.5. ¹H NMR (400 MHz, DMSO-*d*₆) δ 11.30 (s, 1H), 10.93 (s, 1H), 9.11 (s, 1H), 8.94 (d, *J* = 4.8 Hz, 2H), 8.14 (s, 1H), 7.57 (dd, *J* = 7.9, 1.5 Hz, 1H), 7.54–7.49 (m, 2H), 7.30 (t, *J* = 7.9 Hz, 1H), 3.67 (s, 3H), 2.07 (quin, *J* = 6.1 Hz, 1H), 0.85–0.78 (m, 4H).

6-(Cyclopropanecarboxamido)-4-((2-methoxy-3-(5-methylpyrimidin-2-yl)phenyl)amino)-N-(methyl-*d*₃)pyridazine-3-carboxamide (**13**). Yield: 31%. LCMS (ESI) *m/z* calcd for C₂₂H₂₀D₃N₇O₃ (M + H)⁺: 437.2, found: 437.0. ¹H NMR (500 MHz, DMSO-*d*₆) δ 11.33 (s, 1H), 10.94 (s, 1H), 9.14 (s, 1H), 8.79 (s, 2H), 8.16 (s, 1H), 7.56 (d, *J* = 8.1 Hz, 1H), 7.50 (d, *J* = 7.1 Hz, 1H), 7.30 (t, *J* = 7.9 Hz, 1H), 3.66 (s, 3H), 2.35 (s, 3H), 2.08 (quin, *J* = 6.1 Hz, 1H), 0.86–0.80 (m, 4H).

6-(Cyclopropanecarboxamido)-4-((3-(5-fluoropyrimidin-2-yl)-2-methoxyphenyl)amino)-N-(methyl-*d*₃)pyridazine-3-carboxamide (**14**). Yield: 36%. LCMS (ESI) *m/z* calcd for C₂₁H₁₇D₃FN₇O₃ (M + H)⁺: 441.2, found: 441.4. ¹H NMR (500 MHz, DMSO-*d*₆) δ 11.32 (s, 1H), 10.95 (s, 1H), 9.13 (s, 1H), 9.04 (s, 2H), 8.15 (s, 1H), 7.59 (dd, *J* = 7.9, 1.2 Hz, 1H), 7.53 (dd, *J* = 7.8, 1.5 Hz, 1H), 7.32 (t, *J* = 7.9 Hz, 1H), 3.68 (s, 3H), 2.15–2.05 (m, 1H), 0.87–0.80 (m, 4H).

6-(Cyclopropanecarboxamido)-4-((2-methoxy-3-(5-methoxy-pyrimidin-2-yl)phenyl)amino)-N-(methyl-*d*₃)pyridazine-3-carboxamide (**15**). Yield: 36%. LCMS (ESI) *m/z* calcd for C₂₂H₂₀D₃N₇O₄

(M + H)⁺: 453.2, found: 453.4. ¹H NMR (500 MHz, DMSO-*d*₆) δ 11.31 (s, 1H), 10.90 (s, 1H), 9.11 (s, 1H), 8.67 (s, 2H), 8.13 (s, 1H), 7.53 (br d, *J* = 8.1 Hz, 1H), 7.49 (d, *J* = 7.7 Hz, 1H), 7.28 (t, *J* = 7.7 Hz, 1H), 3.97 (s, 3H), 3.64 (s, 3H), 2.12–1.99 (m, 1H), 0.88–0.77 (m, 4H).

6-(Cyclopropanecarboxamido)-4-((2-methoxy-3-(4-methylpyrimidin-2-yl)phenyl)amino)-N-(methyl-*d*₃)pyridazine-3-carboxamide (16). Yield: 31%. LCMS (ESI) *m/z* calcd for C₂₂H₂₀D₃N₇O₃ (M + H)⁺: 437.2, found: 437.4. ¹H NMR (400 MHz, DMSO-*d*₆) δ 11.32 (s, 1H), 10.93 (s, 1H), 9.13 (s, 1H), 8.78 (d, *J* = 5.1 Hz, 1H), 8.15 (s, 1H), 7.57 (dd, *J* = 7.9, 1.5 Hz, 1H), 7.51 (dd, *J* = 7.8, 1.5 Hz, 1H), 7.39 (d, *J* = 5.1 Hz, 1H), 7.33–7.27 (m, 1H), 3.70 (s, 3H), 2.55 (s, 3H), 2.09 (quin, *J* = 6.1 Hz, 1H), 0.83 (d, *J* = 5.9 Hz, 4H).

6-(Cyclopropanecarboxamido)-4-((2-methoxy-3-(4-methoxypyrimidin-2-yl)phenyl)amino)-N-(methyl-*d*₃)pyridazine-3-carboxamide (17). Yield: 33%. LCMS (ESI) *m/z* calcd for C₂₂H₂₀D₃N₇O₄ (M + H)⁺: 453.2, found: 453.3. ¹H NMR (500 MHz, DMSO-*d*₆) δ 11.34 (s, 1H), 10.95 (s, 1H), 9.15 (s, 1H), 8.65 (d, *J* = 5.7 Hz, 1H), 8.15 (s, 1H), 7.58 (d, *J* = 7.7 Hz, 2H), 7.31 (t, *J* = 7.9 Hz, 1H), 6.94 (d, *J* = 5.7 Hz, 1H), 3.99 (s, 3H), 3.72 (s, 3H), 2.17–2.02 (m, 1H), 0.89–0.76 (m, 4H).

6-(Cyclopropanecarboxamido)-4-((3-(5-(2-hydroxypropan-2-yl)pyrimidin-2-yl)-2-methoxyphenyl)amino)-N-(methyl-*d*₃)pyridazine-3-carboxamide (18). Yield: 56%. LCMS (ESI) *m/z* calcd for C₂₄H₂₃D₃N₇O₄ (M + H)⁺: 481.2, found: 481.1. ¹H NMR (400 MHz, DMSO-*d*₆) δ 11.32 (s, 1H), 10.94 (s, 1H), 9.14 (s, 1H), 9.01 (s, 2H), 8.16 (s, 1H), 7.55 (ddd, *J* = 17.5, 7.9, 1.6 Hz, 2H), 7.39–7.24 (m, 1H), 5.45 (s, 1H), 3.70 (s, 3H), 2.15–2.03 (m, 1H), 1.55 (s, 6H), 0.90–0.77 (m, 4H).

6-(Cyclopropanecarboxamido)-4-((3-(5-(dimethylcarbamoyl)pyrimidin-2-yl)-2-methoxyphenyl)amino)-N-(methyl-*d*₃)pyridazine-3-carboxamide (19). Yield: 6%. LCMS (ESI) *m/z* calcd for C₂₄H₂₃D₃N₈O₄ (M + H)⁺: 494.2, found: 494.6. ¹H NMR (400 MHz, DMSO-*d*₆) δ 11.33 (s, 1H), 10.97 (s, 1H), 9.14 (s, 1H), 9.04 (s, 2H), 8.16 (s, 1H), 7.68–7.56 (m, 2H), 7.41–7.27 (m, 1H), 3.71 (s, 3H), 3.06 (s, 6H), 2.16–2.03 (m, 1H), 0.90–0.78 (m, 4H).

6-(Cyclopropanecarboxamido)-4-((2-methoxy-3-(5-(1,1,1-trifluoro-2-hydroxypropan-2-yl)pyrimidin-2-yl)phenyl)amino)-N-(methyl-*d*₃)pyridazine-3-carboxamide (20). Yield: 22%. LCMS (ESI) *m/z* calcd for C₂₄H₂₁D₃F₃N₇O₄ (M + H)⁺: 535.2, found: 535.5. ¹H NMR (400 MHz, DMSO-*d*₆) δ 11.32 (s, 1H), 10.95 (s, 1H), 9.18–9.10 (m, 3H), 8.15 (s, 1H), 7.59 (ddd, *J* = 9.8, 8.0, 1.5 Hz, 2H), 7.33 (t, *J* = 7.9 Hz, 1H), 7.12 (s, 1H), 3.71 (s, 3H), 2.16–2.01 (m, 1H), 1.83 (s, 3H), 0.88–0.78 (m, 4H).

6-(Cyclopropanecarboxamido)-4-((3-(5-(dimethylcarbamoyl)pyrazin-2-yl)-2-methoxyphenyl)amino)-N-(methyl-*d*₃)pyridazine-3-carboxamide (25). Yield: 49%. LCMS (ESI) *m/z* calcd for C₂₄H₂₃D₃N₈O₄ (M + H)⁺: 494.2, found: 494.2. ¹H NMR (400 MHz, DMSO-*d*₆) δ 11.35 (s, 1H), 11.01 (s, 1H), 9.16 (s, 1H), 9.08 (d, *J* = 1.6 Hz, 1H), 8.96 (d, *J* = 1.5 Hz, 1H), 8.17 (s, 1H), 7.63 (ddd, *J* = 7.9, 6.4, 1.5 Hz, 2H), 7.46–7.33 (m, 1H), 3.56 (s, 3H), 3.08 (s, 3H), 3.07 (s, 3H), 2.16–2.05 (m, 1H), 0.89–0.80 (m, 4H).

6-(Cyclopropanecarboxamido)-4-((3-(5-(2-hydroxypropan-2-yl)pyridin-2-yl)-2-methoxyphenyl)amino)-N-(methyl-*d*₃)pyridazine-3-carboxamide (26). Yield: 24%. LCMS (ESI) *m/z* calcd for C₂₅H₂₅D₃N₆O₄ (M + H)⁺: 480.2, found: 480.2. ¹H NMR (400 MHz, DMSO-*d*₆) δ 11.32 (s, 1H), 10.98 (s, 1H), 9.14 (s, 1H), 8.81 (dd, *J* = 2.3, 0.6 Hz, 1H), 8.18 (s, 1H), 7.94 (dd, *J* = 8.2, 2.3 Hz, 1H), 7.81 (d, *J* = 8.3 Hz, 1H), 7.55 (dd, *J* = 7.8, 1.6 Hz, 1H), 7.50 (dd, *J* = 7.9, 1.5 Hz, 1H), 7.33–7.27 (m, 1H), 5.26 (br s, 1H), 3.49 (s, 3H), 2.13–2.06 (m, 1H), 1.51 (s, 6H), 0.83 (d, *J* = 5.9 Hz, 4H).

6-(Cyclopropanecarboxamido)-4-((3-(5-(dimethylcarbamoyl)pyridin-2-yl)-2-methoxyphenyl)amino)-N-(methyl-*d*₃)pyridazine-3-carboxamide (27). Yield: 43%. LCMS (ESI) *m/z* calcd for C₂₅H₂₄D₃N₇O₄ (M + H)⁺: 493.2, found: 493.2. ¹H NMR (500 MHz, DMSO-*d*₆) δ 11.35 (s, 1H), 11.00 (s, 1H), 9.15 (s, 1H), 8.75 (s, 1H), 8.18 (s, 1H), 8.01–7.90 (m, 2H), 7.66–7.48 (m, 2H), 7.34 (t, *J* = 7.7 Hz, 1H), 3.51 (s, 3H), 3.04 (br s, 3H), 3.01 (br s, 3H), 2.14–2.02 (m, 1H), 0.87–0.81 (m, 4H).

6-(Cyclopropanecarboxamido)-4-((3-(6-(dimethylcarbamoyl)pyridazin-3-yl)-2-methoxyphenyl)amino)-N-(methyl-*d*₃)pyridazine-3-carboxamide (29). Yield: 16%. LCMS (ESI) *m/z* calcd for

C₂₄H₂₃D₃N₈O₄ (M + H)⁺: 494.2, found: 494.2. ¹H NMR (500 MHz, DMSO-*d*₆) δ 11.36 (s, 1H), 11.00 (s, 1H), 9.16 (s, 1H), 8.25–8.14 (m, 2H), 7.95 (d, *J* = 8.8 Hz, 1H), 7.64 (dd, *J* = 6.7, 5.4 Hz, 2H), 7.40 (t, *J* = 7.9 Hz, 1H), 3.50 (s, 3H), 3.11 (s, 3H), 3.05 (s, 3H), 2.09 (quin, *J* = 6.1 Hz, 1H), 0.90–0.79 (m, 4H).

5-Fluoro-2-methoxy-3-(4,4,5,5-tetramethyl-1,3,2-dioxaborolan-2-yl)aniline (40). A mixture of 3-bromo-5-fluoro-2-methoxyaniline (39) (0.304 g, 1.382 mmol), 4,4,4',4',5,5,5',5'-octamethyl-2,2'-bi(1,3,2-dioxaborolane) (0.526 g, 2.072 mmol), PdCl₂(dppf)-CH₂Cl₂ adduct (0.068 g, 0.083 mmol), and potassium acetate (0.407 g, 4.14 mmol) in 1,4-dioxane (7 mL) was heated in a pressure bottle at 105 °C for 18 h. The mixture was diluted with ethyl acetate (10 mL) and filtered through Celite. The filtrate was concentrated under vacuum, and the residue was submitted to flash chromatography (40 g ISCO column, solid loading, 0–60% diethyl ether/hexane) to afford the title compound (0.225 g, 0.842 mmol, 61% yield) as a white solid. LCMS (ESI) *m/z* calcd for C₁₃H₁₉BFNO₃ (M + H)⁺: 268.1, found: 268.2. ¹H NMR (400 MHz, chloroform-*d*) δ 6.74 (dd, *J* = 8.7, 3.0 Hz, 1H), 6.53 (dd, *J* = 9.6, 3.1 Hz, 1H), 3.91 (br s, 2H), 3.77 (s, 3H), 1.35 (s, 12H).

Ethyl 2-(3-Amino-2-methoxyphenyl)pyrimidine-5-carboxylate (41a). A solution of 2-methoxy-3-(4,4,5,5-tetramethyl-1,3,2-dioxaborolan-2-yl)aniline (35) (1.508 g, 6.06 mmol), ethyl 2-chloropyrimidine-5-carboxylate (1.244 g, 6.67 mmol), PdCl₂(dppf)-CH₂Cl₂ adduct (0.260 g, 0.319 mmol), and 2 M K₃PO₄ solution (9.0 mL, 18.0 mmol) in 1,4-dioxane (40 mL) in a sealed vial was heated at 75 °C for 4 h. Upon cooling to rt, the mixture was diluted with ethyl acetate (150 mL) and filtered through Celite. The filtrate was washed with brine (40 mL), dried over Na₂SO₄, and concentrated under vacuum. The residue was subjected to flash chromatography (80 g ISCO column, solid loading, 0–75% ethyl acetate/hexane) to afford the title compound (1.288 g, 4.48 mmol, 74% yield) as a slightly yellow oil. LCMS (ESI) *m/z* calcd for C₁₄H₁₅N₃O₃ (M + H)⁺: 274.1, found: 274.3. ¹H NMR (400 MHz, DMSO-*d*₆) δ 9.31 (s, 2H), 6.98–6.93 (m, 2H), 6.91–6.85 (m, 1H), 5.08 (s, 2H), 4.41 (q, *J* = 7.1 Hz, 2H), 3.65 (s, 3H), 1.37 (t, *J* = 7.1 Hz, 3H).

Ethyl 2-(3-Amino-5-fluoro-2-methoxyphenyl)pyrimidine-5-carboxylate (41b). This compound was prepared from 40 in the same manner as 41a from 35. Yield: 79%. LCMS (ESI) *m/z* calcd for C₁₄H₁₄FN₃O₃ (M + H)⁺: 292.1, found: 292.4. ¹H NMR (400 MHz, DMSO-*d*₆) δ 9.32 (s, 2H), 6.73–6.61 (m, 2H), 5.46 (s, 2H), 4.41 (q, *J* = 7.1 Hz, 2H), 3.64 (s, 3H), 1.37 (t, *J* = 7.1 Hz, 3H).

Ethyl 2-(3-((6-Chloro-3-((methyl-*d*₃)carbamoyl)pyridazin-4-yl)amino)-2-methoxyphenyl)pyrimidine-5-carboxylate (42a). To a solution of ethyl 2-(3-amino-2-methoxyphenyl)pyrimidine-5-carboxylate (41a) (0.710 g, 2.60 mmol) and 4,6-dichloro-*N*-(methyl-*d*₃)pyridazine-3-carboxamide (37)⁵³ (0.552 g, 2.64 mmol) in THF (24 mL) at rt was added 1 M lithium bis(trimethylsilyl)amide/THF (8.0 mL, 8.00 mmol) over 3 min. The mixture was stirred at rt for 1.25 h before it was quenched with acetic acid (0.51 mL, 8.91 mmol), diluted with ethyl acetate (150 mL), washed with brine (30 mL), and dried over anhydrous MgSO₄. The desired product (0.366 g, 0.820 mmol, 32% yield) was isolated as a white solid by flash chromatography (40 g ISCO column, 0–50% ethyl acetate/hexane). LCMS (ESI) *m/z* calcd for C₂₀H₁₆D₃ClN₆O₄ (M + H)⁺: 446.2, found: 446.6. ¹H NMR (400 MHz, DMSO-*d*₆) δ 11.13 (s, 1H), 9.38 (s, 3H), 7.79–7.67 (m, 2H), 7.37 (t, *J* = 7.9 Hz, 1H), 7.22 (s, 1H), 4.42 (q, *J* = 7.1 Hz, 2H), 3.70 (s, 3H), 1.38 (t, *J* = 7.1 Hz, 3H).

Ethyl 2-(3-((6-Chloro-3-((methyl-*d*₃)carbamoyl)pyridazin-4-yl)amino)-5-fluoro-2-methoxyphenyl)pyrimidine-5-carboxylate (42b). This compound was prepared from 41b in the same manner as 42a from 41a. Yield: 43%. LCMS (ESI) *m/z* calcd for C₂₀H₁₅D₃ClFN₆O₄ (M + H)⁺: 464.1, found: 464.5. ¹H NMR (400 MHz, DMSO-*d*₆) δ 11.27 (s, 1H), 9.44–9.36 (m, 3H), 7.77–7.68 (m, 1H), 7.52–7.43 (m, 2H), 4.42 (q, *J* = 7.2 Hz, 2H), 3.71 (s, 3H), 1.38 (t, *J* = 7.0 Hz, 3H).

Ethyl 2-(3-((6-(Cyclopropanecarboxamido)-3-((methyl-*d*₃)carbamoyl)pyridazin-4-yl)amino)-2-methoxyphenyl)pyrimidine-5-carboxylate (43a). A mixture of ethyl 2-(3-((6-chloro-3-((methyl-*d*₃)carbamoyl)pyridazin-4-yl)amino)-2-methoxyphenyl)pyrimidine-5-carboxylate (42a) (0.344 g, 0.772

mmol) and cyclopropanecarboxamide (0.131 g, 1.543 mmol), XantPhos (0.067 g, 0.116 mmol), Cs₂CO₃ (0.553 g, 1.697 mmol), and Pd₂(dba)₃ (0.085 g, 0.093 mmol) in 1,4-dioxane (10 mL) was degassed and heated at 150 °C under microwave conditions for 2.5 h. Upon cooling to rt, the mixture was diluted with ethyl acetate (20 mL) and filtered through Celite. To the filtrate was added silica gel (1.7 g), and the mixture was concentrated under vacuum. The residue was subjected to flash chromatography (24 g ISCO column, 25–100% ethyl acetate/hexane) to provide the title compound (0.293 g, 0.556 mmol, 72% yield) as a yellow solid. LCMS (ESI) *m/z* calcd for C₂₄H₂₂D₃N₇O₅ (M + H)⁺: 495.2, found: 495.6. ¹H NMR (400 MHz, DMSO-*d*₆) δ 11.33 (s, 1H), 10.98 (s, 1H), 9.40–9.35 (m, 2H), 9.14 (s, 1H), 8.16 (s, 1H), 7.68–7.61 (m, 2H), 7.35 (t, *J* = 7.9 Hz, 1H), 4.42 (q, *J* = 7.1 Hz, 2H), 3.71 (s, 3H), 2.09 (quin, *J* = 6.2 Hz, 1H), 1.38 (t, *J* = 7.1 Hz, 3H), 0.85–0.81 (m, 4H).

Ethyl 2-(3-((6-(Cyclopropanecarboxamido)-3-((methyl-*d*₃)-carbamoyl)pyridazin-4-yl)amino)-5-fluoro-2-methoxyphenyl)pyrimidine-5-carboxylate (43b). This compound was prepared from 42b in the same manner as 43a from 42a. Yield: 50%. LCMS (ESI) *m/z* calcd for C₂₄H₂₁D₃FN₇O₅ (M + H)⁺: 513.2, found: 513.4. ¹H NMR (400 MHz, DMSO-*d*₆) δ 11.40 (s, 1H), 11.18 (s, 1H), 9.39 (s, 2H), 9.18 (s, 1H), 8.27 (s, 1H), 7.58 (dd, *J* = 9.6, 3.2 Hz, 1H), 7.42 (dd, *J* = 9.0, 3.3 Hz, 1H), 4.42 (q, *J* = 7.0 Hz, 2H), 3.72 (s, 3H), 2.17–2.06 (m, 1H), 1.38 (t, *J* = 7.2 Hz, 3H), 0.91–0.81 (m, 4H).

6-(Cyclopropanecarboxamido)-4-((3-(5-(diethylcarbamoyl)pyrimidin-2-yl)-2-methoxyphenyl)amino)-*N*-(methyl-*d*₃)pyridazine-3-carboxamide (21). To a solution of ethyl 2-(3-((6-(cyclopropanecarboxamido)-3-((methyl-*d*₃)carbamoyl)pyridazin-4-yl)amino)-2-methoxyphenyl)pyrimidine-5-carboxylate (43a) (0.274 g, 0.554 mmol) in methanol (2 mL) and THF (4 mL) at rt was added lithium hydroxide monohydrate (0.122 g, 2.90 mmol) in water (1.5 mL) over 1 min. The mixture was stirred at rt for 1 h and then concentrated under vacuum to a volume of approximately 1.5 mL. The residue was acidified with 1 N hydrochloric acid to pH 4–5. The precipitate was collected by suction filtration and further purified by trituration with ethyl acetate to provide 2-(3-((6-(cyclopropanecarboxamido)-3-((methyl-*d*₃)carbamoyl)pyridazin-4-yl)amino)-2-methoxyphenyl)pyrimidine-5-carboxylic acid (0.170 g, 0.321 mmol, 58% yield). LCMS (ESI) *m/z* calcd for C₂₂H₁₈D₃N₇O₅ (M + H)⁺: 467.2, found: 467.6.

A mixture of 2-(3-((6-(cyclopropanecarboxamido)-3-((methyl-*d*₃)carbamoyl)pyridazin-4-yl)amino)-2-methoxyphenyl)pyrimidine-5-carboxylic acid (0.033 g, 0.070 mmol), diethylamine (0.024 mL, 0.232 mmol), benzotriazol-1-yloxytris(dimethylamino)phosphonium hexafluorophosphate (BOP) (0.0534 g, 0.121 mmol), and diisopropylethylamine (0.06 mL, 0.344 mmol) in THF (1.5 mL) was heated at 50 °C in a sealed vial for 16 h. The mixture was diluted with methanol and injected preparative HPLC. The correct fractions were combined, concentrated under vacuum, basified with saturated NaHCO₃ solution, and extracted with dichloromethane (3 x 30 mL). The combined extract was dried over anhydrous MgSO₄. Removal of the solvent under vacuum afforded the title compound (0.0073 g, 0.014 mmol, 20% yield) as a white solid. LCMS (ESI) *m/z* calcd for C₂₆H₂₇D₃N₈O₄ (M + H)⁺: 522.3, found: 522.7. ¹H NMR (400 MHz, DMSO-*d*₆) δ 11.32 (s, 1H), 10.97 (s, 1H), 9.14 (s, 1H), 9.00 (s, 2H), 8.15 (s, 1H), 7.66–7.56 (m, 2H), 7.34 (t, *J* = 7.9 Hz, 1H), 3.70 (s, 3H), 3.33–3.29 (m, 4H), 2.15–2.03 (m, 1H), 1.22–1.13 (m, 6H), 0.86–0.81 (m, 4H).

6-(Cyclopropanecarboxamido)-4-((3-(5-(dimethylcarbamoyl)pyrimidin-2-yl)-5-fluoro-2-methoxyphenyl)amino)-*N*-(methyl-*d*₃)pyridazine-3-carboxamide (23). This compound was prepared from 43b in the same manner as 21 from 43a. Yield over two steps: 42%. LCMS (ESI) *m/z* calcd for C₂₄H₂₂D₃FN₈O₄ (M + H)⁺: 512.2, found: 512.5. ¹H NMR (500 MHz, DMSO-*d*₆) δ 11.42 (s, 1H), 11.17 (s, 1H), 9.20 (br s, 1H), 9.06 (s, 2H), 8.27 (s, 1H), 7.55 (br d, *J* = 7.0 Hz, 1H), 7.39 (dd, *J* = 9.0, 2.7 Hz, 1H), 3.72 (s, 3H), 3.05 (br s, 3H), 3.04 (br s, 3H), 2.16–2.05 (m, 1H), 0.86 (br d, *J* = 6.1 Hz, 4H).

3-(5-Bromopyrimidin-2-yl)-5-fluoro-2-methoxyaniline (44). A mixture of 5-fluoro-2-methoxy-3-(4,4,5,5-tetramethyl-1,3,2-diox-

borolan-2-yl)aniline (40) (0.785 g, 2.94 mmol), 2,5-dibromopyrimidine (0.734 g, 3.09 mmol), PdCl₂(dppf)-CH₂Cl₂ adduct (0.144 g, 0.176 mmol), and 2 M K₃PO₄ solution (4.41 mL, 8.82 mmol) in 1,4-dioxane (22 mL) was heated at 90 °C for 3 h. The mixture was diluted with ethyl acetate (30 mL) and filtered through Celite. The filtrate was concentrated under vacuum to dryness. The residue was diluted with water (20 mL) and extracted with dichloromethane (4 x 40 mL). The combined extract was dried over anhydrous Na₂SO₄ and concentrated under vacuum. The desired product (0.376 g, 1.261 mmol, 43% yield) was isolated as a pale yellow solid by flash chromatography (80 g ISCO column, 20–50% ethyl acetate/hexane). LCMS (ESI) *m/z* calcd for C₁₁H₉BrFN₃O (M + H)⁺: 298.0, found: 298.0. ¹H NMR (500 MHz, DMSO-*d*₆) δ 9.09 (s, 2H), 6.60 (m, 2H), 5.42 (s, 2H), 3.61 (s, 3H).

3-(5-(1-Ethoxyvinyl)pyrimidin-2-yl)-5-fluoro-2-methoxyaniline (45a). A mixture of 3-(5-bromopyrimidin-2-yl)-5-fluoro-2-methoxyaniline (44) (376 mg, 1.261 mmol), tributyl(1-ethoxyvinyl)stannane (0.457 mL, 1.387 mmol), bis(triphenylphosphine)palladium(II) chloride (26.6 mg, 0.038 mmol), and triethylamine (0.211 mL, 1.514 mmol) in DMF (8 mL) was heated at 100 °C for 16 h. Upon cooling to rt, the mixture was diluted with ethyl acetate (15 mL) and filtered through Celite. The filtrate was further diluted with ethyl acetate (150 mL), washed with water (3 x 35 mL) and brine (35 mL), and dried over anhydrous MgSO₄. Removal of solvent under vacuum provided the title compound (275 mg, 0.950 mmol, 75% yield). This product was used in the next step without further purification. LCMS (ESI) *m/z* calcd for C₁₅H₁₆FN₃O₂ (M + H)⁺: 290.1, found: 290.1.

3-(6-(1-Ethoxyvinyl)pyridazin-3-yl)-2-methoxyaniline (45b). A mixture of 2-methoxy-3-(4,4,5,5-tetramethyl-1,3,2-dioxaborolan-2-yl)aniline (35) (650 mg, 2.61 mmol), 3-chloro-6-(1-ethoxyvinyl)pyridazine (506 mg, 2.74 mmol), PdCl₂(dppf)-CH₂Cl₂ adduct (128 mg, 0.157 mmol), and 2 M K₃PO₄ solution (3.91 mL, 7.83 mmol) in 1,4-dioxane (16 mL) was heated at 105 °C for 16 h. The mixture was diluted with ethyl acetate (20 mL) and filtered through Celite. The filtrate was concentrated under vacuum to dryness. The residue was diluted with water (20 mL) and extracted with dichloromethane (4 x 40 mL). The combined extract was dried over anhydrous MgSO₄ and concentrated under vacuum. The residue was subjected to flash chromatography (80 g ISCO column, 30–70% ethyl acetate/hexane) to provide the title compound (722 mg, 2.66 mmol, 100% yield) as a slightly yellow oil. LCMS (ESI) *m/z* calcd for C₁₅H₁₇N₃O₂ (M + H)⁺: 272.1, found: 272.1.

6-Chloro-4-((3-(5-(1-ethoxyvinyl)pyrimidin-2-yl)-5-fluoro-2-methoxyphenyl)amino)-*N*-(methyl-*d*₃)pyridazine-3-carboxamide (46a). To a solution of 4,6-dichloro-*N*-trideuteromethylpyridazine-3-carboxamide (37)⁵³ (210 mg, 1.00 mmol) and 3-(5-(1-ethoxyvinyl)pyrimidin-2-yl)-5-fluoro-2-methoxyaniline (45a) (275 mg, 0.951 mmol) in THF (10 mL) at rt was added lithium bis(trimethylsilyl)amide in THF (2.57 mL, 2.57 mmol) over 1 min. The mixture was stirred at rt for 1 h before it was quenched with water (3 mL). The resulting mixture was adjusted with 1 N HCl solution to pH 9–10, diluted with ethyl acetate (150 mL), washed with water (2 x 30 mL) and brine (30 mL) successively, and dried over anhydrous MgSO₄. After the solvent was removed under vacuum, the residue was subjected to flash chromatography (40 g ISCO column, solid loading, 25–50% ethyl acetate/dichloromethane) to provide the title compound (329 mg, 0.712 mmol, 75% yield) as a white solid. LCMS (ESI) *m/z* calcd for C₂₁H₁₇D₃ClFN₆O₃ (M + H)⁺: 462.2, found: 462.1.

6-Chloro-4-((3-(6-(1-ethoxyvinyl)pyridazin-3-yl)-2-methoxyphenyl)amino)-*N*-(methyl-*d*₃)pyridazine-3-carboxamide (46b). This compound was prepared from 45b in the same manner as 45a from 44a. Yield: 52%. LCMS (ESI) *m/z* calcd for C₂₁H₁₈D₃ClN₆O₃ (M + H)⁺: 444.2, found: 444.2.

6-(Cyclopropanecarboxamido)-4-((3-(5-(1-ethoxyvinyl)pyrimidin-2-yl)-5-fluoro-2-methoxyphenyl)amino)-*N*-(methyl-*d*₃)pyridazine-3-carboxamide (47a). A mixture of 6-chloro-4-((3-(5-(1-ethoxyvinyl)pyrimidin-2-yl)-5-fluoro-2-methoxyphenyl)amino)-*N*-(methyl-*d*₃)pyridazine-3-carboxamide (46a) (0.329 g, 0.712

mmol), cyclopropanecarboxamide (0.121 g, 1.425 mmol), Pd₂(dba)₃ (0.098 g, 0.107 mmol), XantPhos (0.062 g, 0.107 mmol), and Cs₂CO₃ (0.511 g, 1.567 mmol) in 1,4-dioxane (6 mL) was heated at 150 °C under microwave for 1 h. Upon cooling to rt, the mixture was diluted with ethyl acetate (10 mL) and filtered through Celite. The filtrate was concentrated under vacuum. The residue was subjected to flash chromatography (40 g ISCO column, solid loading, 40–80% ethyl acetate/dichloromethane) to afford the title compound, (0.258 g, 0.505 mmol, 71% yield) as a white solid. LCMS (ESI) *m/z* calcd for C₂₅H₂₃D₃FN₇O₄ (M + H)⁺: 511.2, found: 511.2.

6-(Cyclopropanecarboxamido)-4-((3-(6-(1-ethoxyvinyl)pyridazin-3-yl)-2-methoxyphenyl)amino)-N-(methyl-d₃)-pyridazine-3-carboxamide (47b). This compound was prepared from 46b in the same manner as 47a from 46a. The yield for this step was not calculated because the isolated product was contaminated with 1-methylpyrrolidin-2-one (NMP) (see 48b for a total yield for two steps). LCMS (ESI) *m/z* calcd for C₂₅H₂₄D₃N₇O₄ (M + H)⁺: 493.2, found: 493.2.

4-((3-(5-Acetylpyrimidin-2-yl)-5-fluoro-2-methoxyphenyl)amino)-6-(cyclopropanecarboxamido)-N-(methyl-d₃)-pyridazine-3-carboxamide (48a). To a suspension of 6-(cyclopropanecarboxamido)-4-((3-(5-(1-ethoxyvinyl)pyrimidin-2-yl)-5-fluoro-2-methoxyphenyl)amino)-N-trideuteromethylpyridazine-3-carboxamide (47a) (0.258 g, 0.505 mmol) in THF (20 mL) at rt was added 1 N hydrochloric acid (10 mL, 10.0 mmol). The resulting solution was stirred at rt for 16 h and then concentrated under vacuum to a volume of approximately 10 mL. The residue was basified with 1 N NaOH solution to pH 10. The resulting suspension was allowed to stand at 0 °C for 1 h. The desired product (0.185 g, 0.383 mmol, 76% yield) was collected as a yellow solid by suction filtration and dried at 60 °C under vacuum. LCMS (ESI) *m/z* calcd for C₂₃H₁₉D₃FN₇O₄ (M + H)⁺: 483.2, found: 483.2.

4-((3-(6-Acetylpyridazin-3-yl)-2-methoxyphenyl)amino)-6-(cyclopropanecarboxamido)-N-(methyl-d₃)-pyridazine-3-carboxamide (48b). This compound was prepared from 47b in the same manner as 48a from 47a. Yield: 52% for two steps. LCMS (ESI) *m/z* calcd for C₂₃H₂₀D₃N₇O₄ (M + H)⁺: 465.2, found: 465.3. ¹H NMR (400 MHz, DMSO-*d*₆) δ 11.35 (s, 1H), 11.01 (s, 1H), 9.16 (s, 1H), 8.32–8.25 (m, 1H), 8.24–8.15 (m, 2H), 7.67 (td, *J* = 7.7, 1.5 Hz, 2H), 7.42 (t, *J* = 7.9 Hz, 1H), 3.51 (s, 3H), 2.84 (s, 3H), 2.14–2.05 (m, 1H), 0.84 (d, *J* = 6.1 Hz, 4H).

6-(Cyclopropanecarboxamido)-4-((5-fluoro-3-(5-(2-hydroxypropan-2-yl)pyrimidin-2-yl)-2-methoxyphenyl)amino)-N-(methyl-d₃)-pyridazine-3-carboxamide (22). To a solution of 4-((3-(5-acetylpyrimidin-2-yl)-5-fluoro-2-methoxyphenyl)amino)-6-(cyclopropanecarboxamido)-N-trideuteromethylpyridazine-3-carboxamide (48a) (85 mg, 0.176 mmol) in THF (10 mL) at 0 °C was dropwise added methylmagnesium bromide (0.352 mL, 1.057 mmol). The resulting mixture was stirred at 0 °C for 45 min before it was quenched with water (5 mL). The mixture was diluted with ethyl acetate (120 mL), washed with water (2 x 30 mL) and brine (30 mL) successively, and dried over anhydrous MgSO₄. After the solvent was removed under vacuum, the residue was subjected to preparative HPLC. The correct fractions were combined, concentrated under vacuum, basified with 1.5 M K₂HPO₄ solution to pH 10, and extracted with dichloromethane (3 x 30 mL). The combined extract was dried over anhydrous Na₂SO₄. Removal of the solvent under vacuum provided the title compound (26.0 mg, 0.052 mmol, 29% yield) as a pale solid. LCMS (ESI) *m/z* calcd for C₂₄H₂₃D₃FN₇O₄ (M + H)⁺: 499.2, found: 499.2. LCMS *m/z* = 499.2 (M + H)⁺. ¹H NMR (400 MHz, DMSO-*d*₆) δ 11.40 (s, 1H), 11.13 (s, 1H), 9.18 (s, 1H), 9.03 (s, 2H), 8.26 (s, 1H), 7.50 (dd, *J* = 9.6, 3.1 Hz, 1H), 7.33 (dd, *J* = 9.1, 3.1 Hz, 1H), 5.48 (s, 1H), 3.71 (s, 3H), 2.20–2.01 (m, 1H), 1.55 (s, 6H), 0.93–0.80 (m, 4H).

6-(Cyclopropanecarboxamido)-4-((3-(6-(2-hydroxypropan-2-yl)pyridazin-3-yl)-2-methoxyphenyl)amino)-N-(methyl-d₃)-pyridazine-3-carboxamide (28). This compound was prepared from 48b in the same manner as 22 from 48a. Yield: 38%. LCMS (ESI) *m/z* calcd for C₂₄H₂₄D₃N₇O₄ (M + H)⁺: 481.2, found: 481.2. ¹H NMR (400 MHz, DMSO-*d*₆) δ 11.34 (s, 1H), 11.00 (s, 1H), 9.15 (s, 1H), 8.18 (s, 1H), 8.08–8.03 (m, 1H), 8.00–7.95 (m, 1H), 7.59

(d, *J* = 7.8 Hz, 2H), 7.41–7.34 (m, 1H), 5.53 (s, 1H), 3.49 (s, 3H), 2.10 (quin, *J* = 6.1 Hz, 1H), 1.60 (s, 6H), 0.84 (d, *J* = 6.1 Hz, 4H).

General Procedure for the Preparation of 50a–e, Exemplified by 6-Chloro-4-((3-(5-fluoropyrimidin-2-yl)-2-methoxyphenyl)amino)-N-(methyl-d₃)-nicotinamide (50b). To a solution of 3-(5-fluoropyrimidin-2-yl)-2-methoxyaniline (36 g) (6.67 g, 30.4 mmol) and 4,6-dichloro-N-(methyl-d₃)-nicotinamide (49)⁵³ (6.03 g, 29.0 mmol) in THF (150 mL) at rt was added 1 M lithium bis(trimethylsilyl)amide/THF (90 mL, 90 mmol) over 5 min. The mixture was stirred at rt for 1.5 h before it was quenched by slow addition of water (40 mL). The resulting mixture was adjusted with 1 N hydrochloric acid to pH 9–10 and diluted with ethyl acetate (300 mL). After the layers were separated, the organic layer was washed with water (75 mL) and brine (75 mL) successively, dried over anhydrous Na₂SO₄, and concentrated under vacuum to dryness. The residue was triturated with ethyl acetate to provide the title compound 7.80 g, 19.96 mmol, 69% yield) as a white solid. LCMS (ESI) *m/z* calcd for C₁₈H₁₂D₃ClFN₅O₂ (M + H)⁺: 391.1, found: 391.1. ¹H NMR (400 MHz, DMSO-*d*₆) δ 10.59 (s, 1H), 9.04 (s, 2H), 8.79 (s, 1H), 8.52 (s, 1H), 7.60 (dd, *J* = 7.9, 1.5 Hz, 1H), 7.53 (dd, *J* = 7.7, 1.3 Hz, 1H), 7.35–7.28 (m, 1H), 6.96–6.91 (m, 1H), 3.66 (s, 3H).

6-Chloro-4-((2-methoxy-3-(pyrimidin-2-yl)phenyl)amino)-N-(methyl-d₃)-nicotinamide (50a). Yield: 65%. LCMS (ESI) *m/z* calcd for C₁₈H₁₃D₃ClN₅O₂ (M + H)⁺: 373.1, found: 373.3.

6-Chloro-4-((2-methoxy-3-(5-methylpyrazin-2-yl)phenyl)amino)-N-(methyl-d₃)-nicotinamide (50c). Yield: 64%. LCMS (ESI) *m/z* calcd for C₁₉H₁₅D₃ClN₅O₂ (M + H)⁺: 387.1, found: 387.0.

6-Chloro-4-((2-methoxy-3-(5-methoxypyrazin-2-yl)phenyl)amino)-N-(methyl-d₃)-nicotinamide (50d). Yield: 63%. LCMS (ESI) *m/z* calcd for C₁₉H₁₅D₃ClN₅O₃ (M + H)⁺: 403.1, found: 403.3.

6-Chloro-4-((5-fluoro-2-methoxy-3-(pyrimidin-2-yl)phenyl)amino)-N-(methyl-d₃)-nicotinamide (50e). Yield: 77%. LCMS (ESI) *m/z* calcd for C₁₈H₁₂D₃ClFN₅O₂ (M + H)⁺: 391.1, found: 391.1.

General Procedure for the Preparation of 30–33, Exemplified by 6-(Cyclopropanecarboxamido)-4-((2-methoxy-3-(pyrimidin-2-yl)phenyl)amino)-N-(methyl-d₃)-nicotinamide (30). A mixture of 6-chloro-4-((2-methoxy-3-(pyrimidin-2-yl)phenyl)amino)-N-trideuteromethylnicotinamide (50a) (65 mg, 0.174 mmol), cyclopropanecarboxamide (29.7 mg, 0.349 mmol), Pd₂(dba)₃ (23.95 mg, 0.026 mmol), XantPhos (15.13 mg, 0.026 mmol), and cesium carbonate (125 mg, 0.384 mmol) in 1,4-dioxane (2.2 mL) was heated at 145 °C under microwave conditions for 1 h. The mixture was diluted with ethyl acetate (8 mL) and filtered through Celite. The filtrate was concentrated under vacuum, and the residue was subjected to preparative HPLC. The correct fractions were combined, concentrated under vacuum, basified with saturated NaHCO₃ solution to pH 9–10, and extracted with dichloromethane (3 x 35 mL). The combined extract was dried over anhydrous Na₂SO₄. Removal of the solvent under vacuum provided the title compound (38 mg, 0.089 mmol, 51% yield) as a white solid. LCMS (ESI) *m/z* calcd for C₂₂H₁₉D₃N₆O₃ (M + H)⁺: 422.2, found: 422.3. ¹H NMR (400 MHz, DMSO-*d*₆) δ 10.78 (br s, 1H), 10.66 (s, 1H), 8.95 (d, *J* = 4.9 Hz, 2H), 8.59 (s, 1H), 8.52 (s, 1H), 8.04 (br s, 1H), 7.56 (dd, *J* = 8.0, 1.5 Hz, 1H), 7.51 (t, *J* = 4.9 Hz, 1H), 7.44 (dd, *J* = 7.8, 1.5 Hz, 1H), 7.30–7.24 (m, 1H), 3.68 (s, 3H), 2.04–1.90 (m, 1H), 0.85–0.74 (m, 4H).

6-(Cyclopropanecarboxamido)-4-((2-methoxy-3-(5-methylpyrazin-2-yl)phenyl)amino)-N-(methyl-d₃)-nicotinamide (31). Yield: 45%. LCMS (ESI) *m/z* calcd for C₂₃H₂₁D₃N₆O₃ (M + H)⁺: 436.2, found: 436.0. ¹H NMR (400 MHz, DMSO-*d*₆) δ 10.78 (s, 1H), 10.72 (s, 1H), 8.95 (d, *J* = 1.5 Hz, 1H), 8.70–8.65 (m, 1H), 8.61 (s, 1H), 8.54 (s, 1H), 8.07 (s, 1H), 7.53 (dd, *J* = 7.9, 1.5 Hz, 1H), 7.47 (dd, *J* = 7.8, 1.6 Hz, 1H), 7.34–7.28 (m, 1H), 3.52 (s, 3H), 2.57 (s, 3H), 2.05–1.95 (m, 1H), 0.84–0.75 (m, 4H).

6-(Cyclopropanecarboxamido)-4-((2-methoxy-3-(5-methoxypyrazin-2-yl)phenyl)amino)-N-(methyl-d₃)-nicotinamide (32). Yield: 50%. LCMS (ESI) *m/z* calcd for C₂₃H₂₁D₃N₆O₄ (M + H)⁺: 452.2, found: 452.4. ¹H NMR (500 MHz, DMSO-*d*₆) δ 10.74 (s, 1H), 10.63 (s, 1H), 8.65 (s, 1H), 8.61 (s, 1H), 8.50 (s, 1H), 8.44 (s, 1H), 8.05 (s,

1H), 7.47 (br dd, $J = 12.3, 7.9$ Hz, 2H), 7.33–7.25 (m, 1H), 3.98 (s, 3H), 3.61 (s, 3H), 2.01–1.93 (m, 1H), 0.78 (br d, $J = 5.7$ Hz, 4H).

6-(Cyclopropanecarboxamido)-4-((5-fluoro-2-methoxy-3-(pyrimidin-2-yl)phenyl)amino)-N-(methyl- d_3)nicotinamide (33). Yield: 52%. LCMS (ESI) m/z calcd for $C_{22}H_{18}D_3FN_6O_3$ ($M + H$)⁺: 440.2, found: 440.3. ¹H NMR (400 MHz, DMSO- d_6) δ 10.86 (d, $J = 6.0$ Hz, 2H), 8.97 (d, $J = 4.9$ Hz, 2H), 8.63 (s, 1H), 8.56 (s, 1H), 8.17 (s, 1H), 7.55 (t, $J = 4.9$ Hz, 1H), 7.43 (dd, $J = 10.0, 3.1$ Hz, 1H), 7.22 (dd, $J = 9.1, 3.1$ Hz, 1H), 3.69 (s, 3H), 2.07–1.97 (m, 1H), 0.87–0.77 (m, 4H).

6-(Cyclopropanecarboxamido)-4-((3-(5-fluoropyrimidin-2-yl)-2-methoxyphenyl)amino)-N-(methyl- d_3)nicotinamide (7). 1,4-Dioxane (200 mL) was placed in a N_2 -flushed three-necked 2 L round-bottom flask and bubbled with N_2 for 5 min before $Pd_2(dba)_3$ (2.12 g, 2.316 mmol) and XantPhos (2.68 g, 4.63 mmol) were added. The mixture was stirred with N_2 bubbling for 5 min before 6-chloro-4-((3-(5-fluoropyrimidin-2-yl)-2-methoxyphenyl)amino)-N-(methyl- d_3)nicotinamide (50b) (18.1 g, 46.3 mmol), cyclopropanecarboxamide (7.88 g, 93 mmol), and CS_2CO_3 (37.7 g, 116 mmol) were successively added. The reaction mixture was heated at reflux for 4 h. Upon cooling to 50 °C, the reaction mixture was diluted with ethyl acetate (800 mL), and *N*-acetyl-L-cysteine (15.12 g, 93 mmol) was added. The resulting mixture was stirred at 50 °C for 12 h and then washed with water (800 mL). The aqueous layer was extracted with ethyl acetate (2 x 500 mL). The combined organic phase was dried over anhydrous Na_2SO_4 and concentrated under vacuum. The residue was subjected to flash chromatography (750 g ISCO column, 0–10% MeOH/ CH_2Cl_2). The product thus obtained was dissolved in refluxing EtOH (200 mL) over 1 h. The solution was gradually cooled to –2 °C with an ice/isopropyl alcohol bath. The recrystallized title compound (13.3 g, 30.3 mmol, 65% yield) was collected as a white solid by suction filtration, rinsed with cold EtOH (–20 °C), and dried on a high house vacuum line for 12 h. LCMS (ESI) m/z calcd for $C_{22}H_{18}D_3FN_6O_3$ ($M + H$)⁺: 440.2, found: 440.1. HRMS (ESI) m/z calcd for $C_{22}H_{18}D_3FN_6O_3$ [$M + H$]⁺: 440.18475. Found: 440.19182. ¹H NMR (400 MHz, DMSO- d_6) δ 10.77 (s, 1H), 10.67 (s, 1H), 9.04 (d, $J = 0.9$ Hz, 2H), 8.59 (s, 1H), 8.53 (s, 1H), 8.07 (s, 1H), 7.57 (dd, $J = 7.9, 1.6$ Hz, 1H), 7.43 (dd, $J = 7.7, 1.6$ Hz, 1H), 7.31–7.23 (m, 1H), 3.68 (s, 3H), 2.04–1.94 (m, 1H), 0.82–0.75 (m, 4H). ¹³C NMR (126 MHz, DMSO- d_6) δ 172.7, 167.8, 160.6 (d, $J = 6.4$ Hz, 1C), 156.3 (d, $J = 263.4$ Hz, 1C), 153.9, 151.8, 150.3, 148.5, 145.2 (d, $J = 20.0$ Hz, 2C), 133.3, 132.8, 126.0, 123.8, 123.0, 109.3, 94.8, 61.3, 14.2, 7.6 (s, 2C).

Tyk2/Jak1 JH2 Homogeneous Time-Resolved Fluorescence (HTRF) Assays. Tyk2 JH2 homogeneous time-resolved fluorescence (HTRF) assay was previously described.^{49,53} The Jak1 JH2 HTRF assay was run in exactly the same way as the Tyk2 JH2 HTRF assay except that the His-JAK1 JH2 concentration utilized was 1 nM and the fluorescein-labeled kinase tracer was adjusted to respective K_d for Jak1 JH2.

Protein Production and X-ray Crystallography. Protein production, purification, co-crystallization, and structure determination of Tyk2 JH2 domain (S75–869) in complex with compounds **12** and **29** were carried out as previously reported.^{43,49,50,52,53}

IL-12/IL-18-Induced Serum IFN γ Inhibition in Mice. Compound **7** in 5:5:90 TPGS:EtOH:PEG300 was dosed orally to female C57BL/6 mice (from Charles River Laboratories, age 8–10 weeks) ($n = 8$ /group). One hour later, 0.02 μ g of recombinant rat IL-12 was administered IV. Another hour later following IL-12 administration, 1 μ g of recombinant rat IL-18 was administered IV. Three hours later, blood was collected and serum was obtained by centrifugation for analysis of IFN γ by ELISA.

IL-23-Induced Acanthosis in Mice. To induce acanthosis, recombinant, dual chain, human IL-23 was diluted in sterile phosphate-buffered saline and injected (5 μ g in 20 μ L) into the right ear of C57BL/6 female mice (9 to 11 weeks of age), every other day until the last injection on day 10. Each ear was injected intradermally using a 0.5 cc insulin syringe. A starting “baseline” measurement of the non-injected right ear of each mouse was made on day 0. Thereafter, ear thickness (in thousandths of an inch) was

measured every other day, prior to the next ear injection, using a Mitutoyo dial caliper. Oral dosing with **7** (3, 10, and 30 mg/kg) began approximately 2 h before the first IL-23 injection and continued once daily until day 9, and the study ended on day 11. The compound was formulated as a solution in EtOH:TPGS:PEG300, 5:5:90 vehicle. The placebo/control group was dosed with blank EtOH:TPGS:PEG300, 5:5:90 vehicle. Stelara was administered SC at a dose of 5 mg/kg on day 0.

Anti-CD40 Antibody-Induced Colitis in Mice. The efficacy of **7** was compared with that of the anti-p40 antibody in a p40-dependent model of colitis using B6.CB17-Prkdc^{scid}/SzJ mice. On day –1 and day 4, mice ($n = 10$ /group) were injected with 10 mg/kg anti-p40 antibody, SC. Starting on day 0 and continuing daily through day 5, additional groups of mice ($n = 10$ /group) were dosed with **0** (vehicle control), 10, 25, or 60 mg/kg PO QD **7** in an aqueous suspension vehicle containing 0.5% Methocel (A4M), 0.1% Tween-80 with a final particle size typically ~200–300 nm (d50). Also on day 0, colitis was induced in all five groups with a single injection of 100 μ g of FGK4.5 anti-CD40 mAb in PBS, IP. On a daily basis, mice were weighed and monitored for signs of colitis-including body weight loss and the accompanying loose stools and diarrhea. On day 6, all animals were euthanized. Intestine sections were fixed in formalin or added to RNA later for histological evaluations or cytokine profiling via RT-PCR, respectively. Terminal blood was collected for measuring circulating cytokine levels.

Lupus in NZB/W Mice. Baseline body weight, proteinuria, and serum dsDNA titers were determined for female NZB/W mice, age 23 weeks (Jackson Laboratories) prior to their randomization into treatment groups, each with $n = 12$. Mice were dosed by oral gavage, QD, for 12 weeks and included the following treatment groups: compound **7** at 3 and 10 mg/kg in vehicle (EtOH:TPGS:PEG300, 5:5:90) or vehicle alone. Mouse anti-interferon receptor antibody MARI-5A3 was dosed at 0.5 mg/mouse ($n = 10$), SC, twice a week for the duration of the study. Mice were routinely monitored for overall health, and body weight, proteinuria, and dsDNA titers were measured every 3 weeks, with the last measurement at week 11.

All studies involving animals were conducted in accordance with institutional guidelines as defined by the Institutional Animal Care and Use Committee for U.S. institutions and with the approval of the Bristol-Myers Squibb Animal Care and Use Committee.

■ ASSOCIATED CONTENT

Supporting Information

The Supporting Information is available free of charge at <https://pubs.acs.org/doi/10.1021/acs.jmedchem.0c01698>.

The Molecular formula strings list (CSV) is available free of charge on the ACS Publications website at DOI:

Molecular formula strings list (CSV)

Accession Codes

Atomic coordinates for the X-ray structures of compound **12** (PDB 7K7O) and **29** (PDB 7K7Q) bound to TYK2 JH2 are available from the RCSB Protein Data Bank (www.rcsb.org). Authors will release the atomic coordinates upon article publication.

■ AUTHOR INFORMATION

Corresponding Author

Chunjian Liu – Immunosciences Discovery Chemistry, Bristol-Myers Squibb Research & Development, Princeton, New Jersey 08543, United States; orcid.org/0000-0003-3708-2372; Phone: +1 609 252 6067; Email: chunjian.liu@bma.com

Authors

James Lin – Immunosciences Discovery Chemistry, Bristol-Myers Squibb Research & Development, Princeton, New Jersey 08543, United States

Charles Langevine – Immunosciences Discovery Chemistry, Bristol-Myers Squibb Research & Development, Princeton, New Jersey 08543, United States

Daniel Smith – Department of Discovery Synthesis, Bristol-Myers Squibb Research & Development, Princeton, New Jersey 08543, United States

Jianqing Li – Department of Discovery Synthesis, Bristol-Myers Squibb Research & Development, Princeton, New Jersey 08543, United States; orcid.org/0000-0002-8445-9796

John S. Tokarski – Molecular Structure and Design, Molecular Discovery Technologies, Bristol-Myers Squibb Research & Development, Princeton, New Jersey 08543, United States

Javed Khan – Molecular Structure and Design, Molecular Discovery Technologies, Bristol-Myers Squibb Research & Development, Princeton, New Jersey 08543, United States

Max Ruzanov – Molecular Structure and Design, Molecular Discovery Technologies, Bristol-Myers Squibb Research & Development, Princeton, New Jersey 08543, United States

Joann Strnad – Immunosciences Discovery Biology, Bristol-Myers Squibb Research & Development, Princeton, New Jersey 08543, United States

Adriana Zupa-Fernandez – Immunosciences Discovery Biology, Bristol-Myers Squibb Research & Development, Princeton, New Jersey 08543, United States

Lihong Cheng – Immunosciences Discovery Biology, Bristol-Myers Squibb Research & Development, Princeton, New Jersey 08543, United States

Kathleen M. Gillooly – Immunosciences Discovery Biology, Bristol-Myers Squibb Research & Development, Princeton, New Jersey 08543, United States

David Shuster – Immunosciences Discovery Biology, Bristol-Myers Squibb Research & Development, Princeton, New Jersey 08543, United States

Yifan Zhang – Immunosciences Discovery Biology, Bristol-Myers Squibb Research & Development, Princeton, New Jersey 08543, United States

Anil Thankappan – Immunosciences Discovery Biology, Bristol-Myers Squibb Research & Development, Princeton, New Jersey 08543, United States

Kim W. McIntyre – Immunosciences Discovery Biology, Bristol-Myers Squibb Research & Development, Princeton, New Jersey 08543, United States

Charu Chaudhry – Leads Discovery and Optimization, Bristol-Myers Squibb Research & Development, Princeton, New Jersey 08543, United States

Paul A. Elzinga – Metabolism and Pharmacokinetic Department, Pharmaceutical Candidate Optimization, Bristol-Myers Squibb Research & Development, Princeton, New Jersey 08543, United States

Manoj Chiney – Metabolism and Pharmacokinetic Department, Pharmaceutical Candidate Optimization, Bristol-Myers Squibb Research & Development, Princeton, New Jersey 08543, United States

Anjaneya Chimalakonda – Metabolism and Pharmacokinetic Department, Pharmaceutical Candidate Optimization, Bristol-Myers Squibb Research & Development, Princeton, New Jersey 08543, United States

Louis J. Lombardo – Immunosciences Discovery Chemistry, Bristol-Myers Squibb Research & Development, Princeton, New Jersey 08543, United States; orcid.org/0000-0003-3335-6460

John E. Macor – Immunosciences Discovery Chemistry, Bristol-Myers Squibb Research & Development, Princeton, New Jersey 08543, United States

Percy H. Carter – Immunosciences Discovery Chemistry, Bristol-Myers Squibb Research & Development, Princeton, New Jersey 08543, United States

James R. Burke – Immunosciences Discovery Biology, Bristol-Myers Squibb Research & Development, Princeton, New Jersey 08543, United States

David S. Weinstein – Immunosciences Discovery Chemistry, Bristol-Myers Squibb Research & Development, Princeton, New Jersey 08543, United States

Complete contact information is available at:
<https://pubs.acs.org/10.1021/acs.jmedchem.0c01698>

Notes

The authors declare no competing financial interest.

ACKNOWLEDGMENTS

The authors would like to acknowledge Richard Rampulla and the Department of Discovery Synthesis (DDS) at Biocon Bristol-Myers Squibb Research and Development Center (BBRC) for supplies of some intermediates.

ABBREVIATIONS USED

anti-dsDNA, anti-double stranded deoxyribonucleic acid; Arg, arginine; ATP, adenosine triphosphate; AUC, area under the curve; CD40, cluster of differentiation 40; CIA, collagen-induced arthritis; CL, clearance; EAE, experimental autoimmune encephalomyelitis; C_{max}, maximum concentration; dba, dibenzylideneacetone; DMF, dimethylformamide; DMSO, dimethyl sulfoxide; dppf, 1,1'-bis-(dicyclohexylphosphino)ferrocene; EPO, erythropoietin; F, bioavailability; FDA, Food and Drug Administration; Glu, glutamic acid; HPLC, high-performance liquid chromatography; HRMS, high-resolution mass spectrometry; hWB, human whole blood; Hz, hertz; IBD, inflammatory bowel disease; IC₅₀, half-maximal inhibitory concentration; IFN, interferon; IL, interleukin; IV, intravenous administration; JAK, Janus kinase; JH1, Janus homology 1; JH2, Janus homology 2; LCMS, liquid chromatography–mass spectrometry; LLQ, lower limit of detection; LM, liver microsomal; Lys, lysine; MHz, megahertz; mpk, milligrams per kilogram; mWB, mouse whole blood; NMR, nuclear magnetic resonance; PBMC, peripheral blood mononuclear cell; PD, pharmacodynamic; PDB, Protein Data Bank; PEG, polyethylene glycol; PK, pharmacokinetic; PO, oral administration; PTGS, tocopheryl polyethylene glycol; QD, once-daily administration; RA, rheumatoid arthritis; rt, room temperature; SAR, structure–activity relationships; SCID, severe-combined immunodeficient; SLE, systemic lupus erythematosus; STAT, signal transducer and activator of transcription; TFA, trifluoroacetic acid; THF, tetrahydrofuran; Thr, threonine; TYK2, tyrosine kinase 2; Val, valine; V_{ss}, volume of distribution.

REFERENCES

- (1) Villarino, A. V.; Kanno, Y.; O'Shea, J. J. Mechanisms and Consequences of Jak-STAT Signaling in the Immune System. *Nat. Immunol.* **2017**, *18*, 374–384.
- (2) Sohn, S. J.; Barrett, K.; Abbema, A. V.; Chang, C.; Kohli, P. B.; Kanda, H.; Smith, J.; Lai, Y.; Zhou, A.; Zhang, B.; Yang, W.; Williams, K.; Macleod, C.; Hurley, C. A.; Kulagowski, J. J.; Lewin-Koh, N.; Dengler, H. S.; Johnson, A. R.; Ghilardi, N.; Zak, M.; Liang, J.; Blair, W. S.; Magnuson, S.; Wu, L. C. A Restricted Role for TYK2 Catalytic Activity in Human Cytokine Responses Revealed by Novel TYK2-Selective Inhibitors. *J. Immunol.* **2013**, *191*, 2205–2216.
- (3) Ghoreschi, K.; Laurence, A.; O'Shea, J. J. Janus Kinases in Immune Cell Signaling. *Immunol. Rev.* **2009**, *228*, 273–287.
- (4) Murray, P. J. The JAK-STAT Signaling Pathway: Input and Output Integration. *J. Immunol.* **2007**, *178*, 2623–2629.
- (5) Schindler, C.; Levy, D. E.; Decker, T. JAK-STAT Signaling: From Interferons to Cytokines. *J. Biol. Chem.* **2007**, *282*, 20059–20063.
- (6) Traynor, K. FDA Approves Tofacitinib for Rheumatoid Arthritis. *Am. J. Health Syst. Pharm.* **2012**, *69*, 2120.
- (7) Flanagan, M. E.; Blumenkopf, T. A.; Brissette, W. H.; Brown, M. F.; Casavant, J. M.; Shang-Poa, C.; Doty, J. L.; Elliott, E. A.; Fisher, M. B.; Hines, M.; Kent, C.; Kudlacz, E. M.; Lillie, B. M.; Magnuson, K. S.; McCurdy, S. P.; Munchhof, M. J.; Perry, B. D.; Sawyer, P. S.; Strelevitz, T. J.; Subramanyam, C.; Sun, J.; Whipple, D. A.; Changelian, P. S. Discovery of CP-690,550: A Potent and Selective Janus Kinase (JAK) Inhibitor for the Treatment of Autoimmune Diseases and Organ Transplant Rejection. *J. Med. Chem.* **2010**, *53*, 8468–8484.
- (8) FDA Approves Jakafi (ruxolitinib) to Treat Myelofibrosis. *Drugs.com*. Nov 16, 2011. <https://www.drugs.com/newdrugs/fda-approves-jakafi-myelofibrosis-2949.html> (accessed Nov 8, 2020).
- (9) Campas-Moya, C. Ruxolitinib: Tyrosine-protein Kinase JAK1/2 Inhibitor: Treatment of Myelofibrosis: Treatment of Myeloproliferative Neoplasms: Treatment of Psoriasis. *Drug Future* **2010**, *35*, 457–465.
- (10) Mogul, A.; Corsi, K.; McAuliffe, L. Baricitinib: The Second FDA-Approved JAK Inhibitor for the Treatment of Rheumatoid Arthritis. *Ann. Pharmacother.* **2019**, *53*, 947–953.
- (11) Mayence, A.; Eynde, J. J. V. Baricitinib: A 2018 Novel FDA-Approved Small Molecule Inhibiting Janus Kinases. *Pharmaceuticals* **2019**, *12*, 37.
- (12) Palmer, C. FDA Approves Upadacitinib for Rheumatoid Arthritis. *Rheumatology News*. Aug 16, 2019. <https://www.mdedge.com/rheumatology/article/206593/rheumatoid-arthritis/fda-approves-upadacitinib-rheumatoid-arthritis> (accessed Nov 8, 2020).
- (13) Parmentier, J. M.; Voss, J.; Graff, C.; Schwartz, A.; Argiriadi, M.; Friedman, M.; Camp, H. S.; Padley, R. J.; George, J. S.; Hyland, D.; Rosebraugh, M.; Wishart, N.; Olson, L.; Long, A. J. In Vitro and In Vivo Characterization of the JAK1 Selectivity of Upadacitinib (ABT-494). *BMC Rheumatol.* **2018**, *2*, 23.
- (14) Talpaz, M.; Kiladjian, J.-J. Fedratinib, a Newly Approved Treatment for Patients with Myeloproliferative Neoplasm-associated Myelofibrosis. *Leukemia* **2020**, 1–17.
- (15) Pardanani, A.; Hood, J.; Lasho, T.; Levine, R. L.; Martin, M. B.; Noronha, G.; Finke, C. C.; Mak, C. C.; Mesa, R.; Zhu, H.; Soll, R.; Gilliland, D. G.; Tefferi, A. TG101209, a Small Molecule JAK2-selective Kinase Inhibitor Potently Inhibits Myeloproliferative Disorder-associated JAK2V617F and MPLW515L/K Mutations. *Leukemia* **2007**, *21*, 1658–1668.
- (16) Piskin, G.; Sylva-Steenland, R. M. R.; Bos, J. D.; Teunissen, M. B. M. In vitro and in situ Expression of IL-23 by Keratinocytes in Healthy Skin and Psoriasis lesions: Enhanced Expression in Psoriatic Skin. *J. Immunol.* **2006**, *176*, 1908–1915.
- (17) Lee, E.; Trepicchio, W. L.; Oestreicher, J.; Pittman, D.; Wang, F.; Chamian, F.; Dhodapkar, M.; Krueger, J. G. Increased Expression of Interleukin 23p19 and p40 in Lesional Skin of Patients with Psoriasis Vulgaris. *J. Exp. Med.* **2004**, *199*, 125–130.
- (18) Yawalkar, N.; Karlen, S.; Hunger, R.; Brand, C. U.; Braathen, L. R. Expression of Interleukin-12 is Increased in Psoriatic Skin. *J. Invest. Dermatol.* **1998**, *111*, 1053–1057.
- (19) Tada, Y.; Asahina, A.; Takekoshi, T.; Kishimoto, E.; Mitsui, H.; Saeki, H.; Komine, M.; Tamaki, K. Interleukin 12 Production by Monocytes from Patients with Psoriasis and its Inhibition by Cyclosporin A. *Br. J. Dermatol.* **2006**, *154*, 1180–1183.
- (20) Piskin, G.; Tursen, U.; Sylva-Steenland, R. M. R.; Bos, J. D.; Teunissen, M. B. M. Clinical Improvement in Chronic Plaque-type Psoriasis Lesions after Narrow-band UVB Therapy is Accompanied by a Decrease in the Expression of IFN- γ Inducers - IL-12, IL-18 and IL-23. *Exp. Dermatol.* **2004**, *13*, 764–772.
- (21) Fischer, K.; Przepiera-Będzak, H.; Sawicki, M.; Walecka, A.; Brzosko, I.; Brzosko, M. Serum Interleukin-23 in Polish Patients with Systemic Lupus Erythematosus: Association with Lupus Nephritis, Obesity, and Peripheral Vascular Disease. *Mediators Inflammation* **2017**, 9401432.
- (22) Niewold, T. B.; Clark, D. N.; Salloum, R.; Poole, B. D. Interferon Alpha in Systemic Lupus Erythematosus. *J. Biomed. Biotechnol.* **2010**, 948364.
- (23) Tucci, M.; Lombardi, L.; Richards, H. B.; Dammacco, F.; Silvestris, F. Overexpression of Interleukin-12 and T Helper 1 Predominance in Lupus Nephritis. *Clin. Exp. Immunol.* **2008**, *154*, 247–254.
- (24) Moschen, A. R.; Tilg, H.; Raine, T. IL-12, IL-23 and IL-17 in IBD: Immunobiology and Therapeutic Targeting. *Nat. Rev. Gastroenterol. Hepatol.* **2019**, *16*, 185–196.
- (25) Andreou, N.-P.; Legaki, E.; Gazouli, M. Inflammatory Bowel Disease Pathobiology: the Role of the Interferon Signature. *Ann. Gastroenterol.* **2020**, *33*, 1–9.
- (26) FDA Approves Stelara (ustekinumab) to Treat Psoriasis. *Drugs.com*. Sept 25, 2009. <https://www.drugs.com/newdrugs/fda-approves-stelara-ustekinumab-psoriasis-1667.html> (accessed Nov 8, 2020).
- (27) FDA Approves Stelara (ustekinumab) for the Treatment of Adults with Moderately to Severely Active Crohn's Diseases. *Drugs.com*. Sept 26, 2016. <https://www.drugs.com/newdrugs/fda-approves-stelara-ustekinumab-adults-moderately-severely-active-crohn-s-4436.html> (accessed Nov 8, 2020).
- (28) Boxler, D. Ustekinumab Gains FDA Approval as Ulcerative Colitis Treatment. *Drug Topics*. Oct 23, 2019. <https://www.drugtopics.com/view/ustekinumab-gains-fda-approval-ulcerative-colitis-treatment> (accessed Nov 8, 2020).
- (29) Morand, E. F.; Furie, R.; Tanaka, Y.; Bruce, I. N.; Askanase, A. D.; Richez, C.; Bae, S. C.; Brohawn, P. Z.; Pineda, L.; Berglund, A.; Tummala, R. Trial of Anifrolumab in Active Systemic Lupus Erythematosus. *N. Engl. J. Med.* **2020**, *382*, 211–221.
- (30) Ortmann, R.; Smeltz, R.; Yap, G.; Sher, A.; Shevach, E. M. A Heritable Defect in IL-12 Signaling in B10.Q/J Mice. I. In vitro Analysis. *J. Immunol.* **2001**, *166*, 5712–5719.
- (31) Oyamada, A.; Ikebe, H.; Itsumi, M.; Saiwai, H.; Okada, S.; Shimoda, K.; Iwakura, Y.; Nakayama, K. I.; Iwamoto, Y.; Yoshikai, Y.; Yamada, H. Tyrosine Kinase 2 Plays Critical Roles in the Pathogenic CD4 T Cell Responses for the Development of Experimental Autoimmune Encephalomyelitis. *J. Immunol.* **2009**, *183*, 7539–7546.
- (32) Dendrou, C. A.; Cortes, A.; Shipman, L.; Evans, H. G.; Attfield, K. E.; Jostins, L.; Barber, T.; Kaur, G.; Kuttikkatte, S. B.; Leach, O. A.; Desel, C.; Faergeman, S. L.; Cheeseman, J.; Neville, M. J.; Sawcer, S.; Compston, A.; Johnson, A. R.; Everett, C.; Bell, J. I.; Karpe, F.; Ullsch, M.; Eigenbrot, C.; McVean, G.; Fugger, L. Resolving TYK2 Locus Genotype-to-phenotype Differences in Autoimmunity. *Sci. Transl. Med.* **2016**, *8*, 363ra149.
- (33) Liang, Y.; Zhu, Y.; Xia, Y.; Peng, H.; Yang, X.-K.; Liu, Y.-Y.; Xu, W.-D.; Pan, H.-F.; Ye, D.-Q. Therapeutic Potential of Tyrosine Kinase 2 in Autoimmunity. *Expert Opin. Ther. Targets* **2014**, *18*, 571–580.
- (34) He, X.; Chen, X.; Zhang, H.; Xie, T.; Ye, X.-Y. Selective Tyk2 Inhibitors as Potential Therapeutic Agents: a Patent Review (2015–2018). *Expert Opin. Ther. Pat.* **2019**, *29*, 137–149.

- (35) Weinstein, D. W.; Moslin, R. M. Advances in the Discovery and Development of Selective Tyrosine Kinase 2 (TYK2) Inhibitors. *Med. Chem. Rev.* **2018**, *53*, 177–200.
- (36) Toms, A. V.; Deshpande, A.; McNally, R.; Jeong, Y.; Rogers, J. M.; Kim, C. U.; Gruner, S. M.; Ficarro, S. B.; Marto, J. A.; Sattler, M.; et al. Structure of a Pseudokinase Domain Switch that Controls Oncogenic Activation of Jak Kinases. *Nat. Struct. Mol. Biol.* **2014**, *20*, 1221–1223.
- (37) Min, X.; Ungureanu, D.; Maxwell, S.; Hammarén, H.; Thibault, S.; Hillert, E.-K.; Ayres, M.; Greenfield, B.; Eksterowicz, J.; Gabel, C.; Walker, N.; Silvennoinen, O.; Wang, Z. Structural and Functional Characterization of the JH2 Pseudokinase Domain of JAK Family Tyrosine Kinase 2 (TYK2). *J. Biol. Chem.* **2015**, *290*, 27261–27270.
- (38) Liang, J.; van Abbema, A.; Balazs, M.; Barrett, K.; Berezukovsky, L.; Blair, W.; Chang, C.; Delarosa, D.; DeVoss, J.; Driscoll, J.; Eigenbrot, C.; Ghilardi, N.; Gibbons, P.; Halladay, J.; Johnson, A.; Kohli, P. B.; Lai, Y.; Liu, Y.; Lyssikatos, J.; Mantik, P.; Menghrajani, K.; Murray, J.; Peng, I.; Sambrone, A.; Shia, S.; Shin, Y.; Smith, J.; Sohn, S.; Tsui, V.; Ultsch, M.; Wu, L. C.; Xiao, Y.; Yang, W.; Young, J.; Zhang, B.; Zhu, B.-y.; Magnuson, S. Lead Optimization of a 4-Aminopyridine Benzamide Scaffold To Identify Potent, Selective, and Orally Bioavailable TYK2 Inhibitors. *J. Med. Chem.* **2013**, *56*, 4521–4536.
- (39) Yogo, T.; Nagamiya, H.; Seto, M.; Sasaki, S.; Shih-Chung, H.; Ohba, Y.; Tokunaga, N.; Lee, G. N.; Rhim, C. Y.; Yoon, C. H.; Cho, S. Y.; Skene, R.; Yamamoto, S.; Satou, Y.; Kuno, M.; Miyazaki, T.; Nakagawa, H.; Okabe, A.; Marui, S.; Aso, K.; Yoshida, M. Structure-based Design and Synthesis of 3-Amino-1,5-dihydro-4H-pyrazolopyridin-4-one Derivatives as Tyrosine Kinase 2 Inhibitors. *J. Med. Chem.* **2016**, *59*, 733–749.
- (40) Fensome, A.; Ambler, C. M.; Arnold, E.; Banker, M. E.; Brown, M. F.; Chrencik, J.; Clark, J. D.; Dowty, M. E.; Efremov, I. V.; Flick, A.; Gerstenberger, B. S.; Gopalsamy, A.; Hayward, M. M.; Hegen, M.; Hollingshead, B. D.; Jussif, J.; Knafels, J. D.; Limburg, D. C.; Lin, D.; Lin, T. H.; Pierce, B. S.; Saiah, E.; Sharma, R.; Symanowicz, P. T.; Telliez, J.-B.; Trujillo, J. I.; Vajdos, F. F.; Vincent, F.; Wan, Z.-K.; Xing, L.; Yang, X.; Zhang, L. Dual Inhibition of TYK2 and JAK1 for the Treatment of Autoimmune Diseases: Discovery of ((S)-2,2-Difluorocyclopropyl)((1R,5S)-3-((1-methyl-1H-pyrazol-4-yl)-amino)-pyrimidin-4-yl)-3,8-diazabicyclo[3.2.1]octan-8-yl)methanone (PF-06700841). *J. Med. Chem.* **2018**, *61*, 8597–8612.
- (41) Banfield, C.; Scaramozza, M.; Zhang, W.; Kieras, E.; Page, K. M.; Fensome, A.; Vincent, M.; Dowty, M. E.; Goteti, K.; Winkle, P. J.; Peeva, E. The Safety, Tolerability, Pharmacokinetics, and Pharmacodynamics of a TYK2/JAK1 Inhibitor (PF-06700841) in Healthy Subjects and Patients with Plaque Psoriasis. *J. Clin. Pharmacol.* **2018**, *58*, 434–447.
- (42) Gerstenberger, B. S.; Ambler, C.; Arnold, E. P.; Banker, M.-E.; Brown, M. F.; Clark, J. D.; Dermenci, A.; Dowty, M. E.; Fensome, A.; Fish, S.; Hayward, M. M.; Hegen, M.; Hollingshead, B. D.; Knafels, J. D.; Lin, D. W.; Lin, T. H.; Owen, D. R.; Saiah, E.; Sharma, R.; Vajdos, F. F.; Xing, L.; Yang, X.; Wright, S. W. Discovery of Tyrosine Kinase 2 (TYK2) Inhibitor (PF-06826647) for the Treatment of Autoimmune Diseases. *J. Med. Chem.* **2020**, 13561.
- (43) Tokarski, J. S.; Zupa-Fernandez, A.; Tredup, J. A.; Pike, K.; Chang, C. Y.; Xie, D.; Cheng, L.; Pedicord, D.; Muckelbauer, J.; Johnson, S. R.; Wu, S.; Edavettal, S. C.; Hong, Y.; Witmer, M. R.; Elkin, L. L.; Blat, Y.; Pitts, W. J.; Weinstein, D. S.; Burke, J. R. Tyrosine Kinase 2-mediated Signal Transduction in T Lymphocytes is Blocked by Pharmacological Stabilization of its Pseudokinase Domain. *J. Biol. Chem.* **2015**, *290*, 11061–11074.
- (44) Lupardus, P. J.; Ultsch, M.; Wallweber, H.; Bir Kohli, P.; Johnson, A. R.; Eigenbrot, C. Structure of the Pseudokinase-Kinase Domains from Protein Kinase TYK2 Reveals a Mechanism for Janus Kinase (JAK) Autoinhibition. *Proc. Natl. Acad. Sci.* **2014**, *111*, 8025–8030.
- (45) Toms, A. V.; Deshpande, A.; McNally, R.; Jeong, Y.; Rogers, J. M.; Kim, C. U.; Gruner, S. M.; Ficarro, S. B.; Marto, J. A.; Sattler, M.; Griffin, J. D.; Eck, M. J. Structure of a Pseudokinase Domain Switch that Controls Oncogenic Activation of Jak Kinases. *Nat. Struct. Mol. Biol.* **2013**, *20*, 1221–1223.
- (46) Bandaranayake, R. M.; Ungureanu, D.; Shan, Y.; Shaw, D. E.; Silvennoinen, O.; Hubbard, S. R. Crystal Structures of the JAK2 Pseudokinase Domain and the Pathogenic Mutant V617F. *Nat. Struct. Mol. Biol.* **2012**, *19*, 754–759.
- (47) Staerk, J.; Kallin, A.; Demoulin, J. B.; Vainchenker, W.; Constantinescu, S. N. JAK1 and Tyk2 Activation by the Homologous Polycythemia Vera JAK2 V617F Mutation: Cross-talk with IGF1 Receptor. *J. Biol. Chem.* **2005**, *280*, 41893–41899.
- (48) Byrne, D. P.; Foulkes, D. M.; Evers, P. A. Pseudokinases: Update on their Functions and Evaluation as New Drug Targets. *Future Med. Chem.* **2017**, *9*, 245–265.
- (49) Liu, C.; Lin, J.; Moslin, R.; Tokarski, J. S.; Muckelbauer, J.; Chang, C.; Tredup, J.; Xie, D.; Park, H.; Li, P.; Wu, D.-R.; Strnad, J.; Zupa-Fernandez, A.; Cheng, L.; Chaudhry, C.; Chen, J.; Chen, C.; Sun, H.; Elzinga, P.; D'Arienzo, C.; Gillooly, K.; Taylor, T. L.; McIntyre, K. W.; Salter-Cid, L.; Lombardo, L. J.; Carter, P. H.; Aranibar, N.; Burke, J. R.; Weinstein, D. S. Identification of Imidazo[1,2-b]pyridazine Derivatives as Potent, Selective, and Orally Active Tyk2 JH2 Inhibitors. *ACS Med. Chem. Lett.* **2019**, *10*, 383–388.
- (50) Wroblewski, S. T.; Moslin, R.; Lin, S.; Zhang, Y.; Spergel, S.; Kempson, J.; Tokarski, J. S.; Strnad, J.; Zupa-Fernandez, A.; Cheng, L.; Shuster, D.; Gillooly, K.; Yang, X.; Heimrich, E.; McIntyre, K. W.; Chaudhry, C.; Khan, J.; Ruzanov, M.; Tredup, J.; Mulligan, D.; Xie, D.; Sun, H.; Huang, C.; D'Arienzo, C.; Aranibar, N.; Chiney, M.; Chimalakonda, A.; Pitts, W. J.; Lombardo, L.; Carter, P. H.; Burke, J. R.; Weinstein, D. S. Highly Selective Inhibition of Tyrosine Kinase 2 (TYK2) for the Treatment of Autoimmune Diseases: Discovery of the Allosteric Inhibitor BMS-986165. *J. Med. Chem.* **2019**, *62*, 8973–8995.
- (51) Burke, J. R.; Cheng, L.; Gillooly, K. M.; Strnad, J.; Zupa-Fernandez, A.; Catlett, I. M.; Zhang, Y.; Heimrich, E. M.; McIntyre, K. W.; Cunningham, M. D.; Carman, J. A.; Zhou, X.; Banas, D.; Chaudhry, C.; Li, S.; D'Arienzo, C.; Chimalakonda, A.; Yang, X.; Xie, J. H.; Pang, J.; Zhao, Q.; Rose, S. M.; Huang, J.; Moslin, R. M.; Wroblewski, S. T.; Weinstein, D. S.; Salter-Cid, L. M. Autoimmune Pathways in Mice and Humans are Blocked by Pharmacological Stabilization of the TYK2 Pseudokinase Domain. *Sci. Transl. Med.* **2019**, *11*, eaaw1736.
- (52) Papp, K.; Gordon, K.; Taçi, D.; Morita, A.; Gooderham, M.; Foley, P.; Girgis, I. G.; Kundu, S.; Banerjee, S. Phase 2 Trial of Selective Tyrosine Kinase 2 Inhibition in Psoriasis. *N. Engl. J. Med.* **2018**, *379*, 1313–1321.
- (53) Moslin, R.; Zhang, Y.; Wroblewski, S. T.; Lin, S.; Mertzman, M.; Spergel, S.; Tokarski, J. S.; Strnad, J.; Gillooly, K.; McIntyre, K. W.; Zupa-Fernandez, A.; Cheng, L.; Sun, H.; Chaudhry, C.; Huang, C.; D'Arienzo, C.; Heimrich, E.; Yang, X.; Muckelbauer, J. K.; Chang, C.; Tredup, J.; Mulligan, D.; Xie, D.; Aranibar, N.; Chiney, M.; Burke, J. R.; Lombardo, L.; Carter, P. H.; Weinstein, D. S. Identification of N-Methyl Nicotinamide and N-Methyl Pyridazine-3-carboxamide Pseudokinase Domain Ligands as Highly Selective Inhibitors of Tyrosine Kinase 2 (TYK2). *J. Med. Chem.* **2019**, *62*, 8953–8972.
- (54) PDB ID: 7K7O
- (55) PDB ID: 7K7Q
- (56) Theofilopoulos, A. N.; Dixon, F. J. Murine Models of Systemic Lupus Erythematosus. *Adv. Immunol.* **1985**, *37*, 269–390.
- (57) Liu, C.; Lin, J.; Moslin, R. M.; Weinstein, D. S.; Tokarski, J. S. Imidazopyridazine Compounds Useful as Modulators of IL-12, IL-23 and/or IFN-alpha Responses. U.S. Patent 10,273,237, April 30, 2019.